

1       **Directing Visceral White Adipocyte Precursors to a Thermogenic**  
2       **Adipocyte Fate Improves Insulin Sensitivity in Obese Mice**  
3

4 Chelsea Hepler, Mengle Shao, Jonathan Y. Xia, Alexandra L. Ghaben, Mackenzie J.  
5 Pearson, Lavanya Vishvanath, Ankit X. Sharma, Thomas S. Morley, William L. Holland,  
6 Rana K. Gupta

7 Touchstone Diabetes Center, Department of Internal Medicine, University of Texas  
8 Southwestern Medical Center, Dallas, Texas 75390, USA  
9

10 Correspondence should be addressed to:

11 Rana K. Gupta

12 Touchstone Diabetes Center

13 Department of Internal Medicine

14 UT Southwestern Medical Center

15 5323 Harry Hines Blvd.

16 K5.240

17 Dallas, TX 75390-8549

18 Phone: 214-648-8721

19 Email: Rana.Gupta@UTSouthwestern.edu

20 **Conflicting interests statement.** The authors declare that they have no competing  
21 financial interests.  
22

## Abstract

Visceral adiposity confers significant risk for developing metabolic disease in obesity whereas preferential expansion of subcutaneous white adipose tissue (WAT) appears protective. Unlike subcutaneous WAT, visceral WAT is resistant to adopting a protective thermogenic phenotype characterized by the accumulation of Ucp1<sup>+</sup> beige/BRITE adipocytes (termed “browning”). In this study, we investigated the physiological consequences of browning murine visceral WAT by selective genetic ablation of *Zfp423*, a transcriptional suppressor of the adipocyte thermogenic program. *Zfp423* deletion in fetal visceral adipose precursors (*Zfp423*<sup>loxP/loxP</sup>; *Wt1-Cre*), or adult visceral white adipose precursors (*Pdgfrb*<sup>rtTA</sup>; *TRE-Cre*; *Zfp423*<sup>loxP/loxP</sup>), results in the accumulation of beige-like thermogenic adipocytes within multiple visceral adipose depots. Thermogenic visceral WAT improves cold tolerance and prevents and reverses insulin resistance in obesity. These data indicate that beneficial visceral WAT browning can be engineered by directing visceral white adipocyte precursors to a thermogenic adipocyte fate, and suggest a novel strategy to combat insulin resistance in obesity.

## Introduction

Adipocytes are critical regulators of energy balance and nutrient homeostasis. White adipocytes serve as the principle site for energy storage in mammals. These cells are characterized by a large unilocular lipid droplet and have the capacity to store or release energy depending on metabolic demand. White adipocytes also produce and secrete numerous cytokines and hormones that impact several aspects of physiology (Rosen and Spiegelman, 2014). Eutherian mammals also contain a second major class of adipocytes that function to catabolize stored lipids and produce heat. These thermogenic adipocytes, consisting of brown and beige/BRITE adipocytes, are characterized by their multilocular lipid droplet appearance, high mitochondrial content, and expression of *uncoupling protein 1* (Ucp1) (Cohen and Spiegelman, 2015; Harms and Seale, 2013). Brown/beige adipocytes have promising therapeutic potential as their activation in the setting of obesity has a profound impact on metabolic health.

White adipose depots are broadly categorized as either subcutaneous or visceral adipose tissue, reflecting their anatomical location. Adipose tissue distribution is a strong predictor of metabolic outcome in obese individuals (Karpe and Pinnick, 2015; Lee et al., 2013). Visceral adiposity strongly correlates with the development of insulin resistance, diabetes, and cardiovascular disease (Kissebah et al., 1982; Krotkiewski et al., 1983; Ohlson et al., 1985; Vague, 1956). Preferential expansion of subcutaneous depots is associated with sustained insulin sensitivity (Manolopoulos et al., 2010). Engineered rodent models highlight the protective role of subcutaneous adipose tissue. Transgenic animals overexpressing *adiponectin* or *mitoNEET* develop extreme subcutaneous obesity; however, these animals remain metabolically healthy (Kim et al., 2007; Kusminski et al., 2012).

In humans, the location of visceral adipose tissue itself likely mediates some of its detrimental effects on energy metabolism; lipids, metabolites, and cytokines can drain directly into the portal circulation and affect liver function (Rytka et al., 2011). Transplantation studies, cellular studies, and gene expression analyses, suggest that factors intrinsic to these depots may also determine their effect on nutrient homeostasis (Tran et al., 2008; Yamamoto et al., 2010). Anatomically distinct adipocytes are functionally unique, differing in their ability to undergo lipolysis, lipogenesis, and activate the thermogenic gene program (Lee et al., 2013; Macotela et al., 2012; Morgan-Bathke et al., 2015; Wu et al., 2012). Along these lines, lineage analyses reveal that anatomically distinct white adipocytes can originate from developmentally distinct precursor cells, and emerge at different times during development (Billon and Dani, 2012; Chau et al., 2014). As such, it is now widely believed that visceral and subcutaneous adipocytes represent distinct subtypes of fat cells.

In mice, visceral and subcutaneous white adipose depots differ remarkably in their ability to remodel under physiological conditions (Hepler and Gupta, 2017). Upon high-fat diet feeding, visceral adipose depots of mice expand by both adipocyte hypertrophy and through the formation of new adipocytes (“adipogenesis”) (Wang et al., 2013). Inguinal subcutaneous WAT expands predominantly through adipocyte hypertrophy. The differential capacity for adipogenesis is likely explained by factors present in the local microenvironment (Jeffery et al., 2016). Another notable difference between the inguinal and visceral adipose depots in rodents is the capacity to adopt a thermogenic phenotype. Various stimuli, including  $\beta$ 3-adrenergic receptor-agonism and cold exposure, drive the rapid accumulation of beige adipocytes in subcutaneous



depots (Vitali et al., 2012; Wu et al., 2012). Genetic stimulation of subcutaneous beige adipogenesis renders mice resistant to high-fat diet induced obesity and/or diabetes (Seale et al., 2011; Shao et al., 2016), while inhibition of subcutaneous beiging leads to an earlier onset of insulin resistance during obesity (Cohen et al., 2014). Most visceral depots in mice, particularly the gonadal and mesenteric adipose tissues, are relatively resistant to browning in response to physiological stimuli. With few exceptions (Kiefer et al., 2012), most engineered mouse models of white adipose tissue browning exhibit beige cell accumulation preferentially in subcutaneous WAT depots (Seale et al., 2011; Stine et al., 2016). Visceral WAT depots may harbor mechanisms to suppress thermogenesis in order to ensure its function as a white, energy-storing, depot.

We previously established a critical role for the transcription factor, *Zfp423*, in the establishment and maintenance of the adipocyte lineage. *Zfp423* is required for fetal differentiation of subcutaneous white adipocytes (Gupta et al., 2010; Shao et al., 2017). In adult mice, *Zfp423* expression defines a subset of committed mural preadipocytes (Gupta et al., 2012; Vishvanath et al., 2016). Upon high-fat diet feeding, these mural cells undergo adipogenesis in visceral depots, contributing to adipocyte hyperplasia (Vishvanath et al., 2016). *Zfp423* is also expressed in nearly all mature adipocytes; however, its expression is more abundant in white adipocytes than brown adipocytes (Shao et al., 2016). In the mature adipocyte, *Zfp423* acts to maintain the energy-storing status of the white adipocyte through suppression of the thermogenic gene program (Shao et al., 2016). *Zfp423* likely exerts this function by serving as a transcriptional co-repressor of the brown/beige lineage determining transcription factor, *Ebf2*. The loss of *Zfp423* in mature white adipocytes triggers a robust conversion of white to beige

adipocytes in subcutaneous WAT. Amongst the various adipose tissues, visceral WAT expresses the highest levels of *Zfp423*. Importantly, we observed that visceral adipocytes lacking *Zfp423* were also capable of inducing their thermogenic gene program when animals were stimulated pharmacologically with a  $\beta 3$  adrenergic receptor agonist (Shao et al., 2016). This observation affords the possibility of examining whether the thermogenic capacity of visceral white adipose depots can be unlocked under physiological conditions, and whether thermogenic visceral WAT would be ultimately harmful or beneficial to systemic metabolic health.

Here, we describe two mouse models of visceral adipose tissue browning derived through selective ablation of *Zfp423* in visceral adipose precursors. We reveal that fetal visceral white preadipocytes can be redirected to a beige-like adipocyte fate through the loss of *Zfp423*, leading to visceral depot mass reduction and fat redistribution towards subcutaneous depots. The browning of visceral depots improves cold tolerance and protects against the development of insulin resistance and hyperlipidemia in obesity. Moreover, we demonstrate that visceral mural preadipocytes in adult mice can also be directed to a thermogenic cell fate; this leads to beige-like, rather than white, adipocyte hyperplasia, in the expanding visceral WAT depots of diet-induced obese animals. Upon activation by  $\beta$ -3 adrenergic receptor agonism, these beige-like adipocytes can trigger an amelioration of insulin resistance in obese animals. Together, these data establish *Zfp423* as a physiological suppressor of the thermogenic gene program in visceral WAT and provide proof of concept that the thermogenic capacity of visceral WAT can be induced under physiological conditions through removal of this molecular brake on the thermogenic gene program in adipose

133 precursors. These data also highlight the potential of visceral WAT, much like  
134 subcutaneous WAT, to improve nutrient homeostasis in obesity when a thermogenic  
135 beige-like phenotype is induced.

## Results

### Selective ablation of *Zfp423* in fetal visceral white adipocyte precursors leads to the formation of thermogenic visceral adipose depots.

We hypothesized that the thermogenic capacity of visceral white adipose depots can be unlocked under physiological conditions through removal of *Zfp423*, and that engineered visceral thermogenic adipocytes can drive improvements in systemic metabolic health. To test this, we derived a mouse model in which *Zfp423* is selectively inactivated in visceral, but not subcutaneous, WAT depots or classic brown adipose tissue depots (BAT). These animals were generated by breeding transgenic mice expressing Cre recombinase under the control of the *Wilms Tumor 1* locus (*Wt1-Cre*) to animals carrying the floxed *Zfp423* alleles (*Zfp423*<sup>loxP/loxP</sup>) (Figure 1A) (*Zfp423*<sup>loxP/loxP</sup>; *Wt1-Cre* animals, herein “Vis-KO” mice). *Wt1-Cre* mice targets *Wt1*-expressing cells of the embryonic mesothelium, as well as descending cells, which include, adult mesothelial cells and intra-abdominal stromal cells within or surrounding visceral organs. Hastie and colleagues revealed that visceral white adipocytes, but not subcutaneous or classic brown adipocytes, descend from *Wt1*-expressing progenitors and are targeted by *Wt1-Cre* (Chau et al., 2014). Specifically, *Wt1-Cre* targets the majority of gonadal adipocyte precursors and variable numbers of precursors in other visceral depots, including the mesenteric and retroperitoneal depots. Analysis of mRNA expression from multiple fat depots in Vis-KO mice confirmed the deletion of *Zfp423* was selective to visceral WAT depots (Figure 1B).

Vis-KO mice were born in the expected Mendelian ratio and appeared grossly indistinguishable from controls. We did not observe a difference in body weight between

eight weeks-old Vis-KO mice and littermate controls; however, we did observe a noticeable difference in body fat distribution (Figure 1C). In comparison to control animals, Vis-KO mice had smaller gonadal WAT depots and larger subcutaneous inguinal WAT (Figure 1D). mRNA levels of adipocyte-selective genes in visceral adipose depots from the Vis-KO were comparable to levels found in control animals (Figure 1E); these data suggest that visceral adipocyte differentiation *per se* does not depend on *Zfp423*. However, in all visceral depots examined, there was a marked increase in the expression of key genes involved in adipocyte thermogenesis, including *Ucp1* (Figure 1F-G). This was accompanied by an increase in basal O<sub>2</sub> consumption rates in explanted WAT depots (Figure 1H-J). Furthermore, some visceral depots (mesenteric and retroperitoneal) lacking *Zfp423* exhibit a multilocular appearance typical of thermogenic adipocytes (Figure 1L-O, Figure 1- figure supplement 1A-L). Taken together, these results indicate that inactivation of *Zfp423* in fetal visceral white adipocyte precursors leads to the widespread accumulation of beige-like thermogenic adipocytes within visceral adipose depots. Interestingly, despite the fact that *Zfp423* was not inactivated in the subcutaneous inguinal WAT of Vis-KO animals, the thermogenic capacity of this depot was also enhanced (Figure 1F,G, K).

***Zfp423*-deficient visceral adipose precursors differentiate into functional thermogenic adipocytes *in vitro*.**

We next asked whether the browning of WAT depots in the Vis-KO animals may occur in a cell-autonomous manner. We isolated the adipose stromal vascular fraction (SVF) from control and Vis-KO mice and performed *in vitro* adipocyte differentiation assays. SVF cultures obtained from the inguinal WAT of control and Vis-KO animals differentiated to a similar degree, and no significant differences in levels of *Zfp423* or

thermogenic genes were observed (Figure 2A-C). This is consistent with lack of Cre activity in this depot, and suggests that the increased inguinal WAT being in Vis-KO mice *in vivo* occurs secondary to inactivation of *Zfp423* in the *Wt1* lineage.

Cultures of gonadal WAT SVF from control and mutant animals also underwent adipogenesis to a similar degree under the differentiation conditions utilized (dexamethasone, IMBX, insulin, and rosiglitazone). This was evident by comparable lipid accumulation and mRNA levels of adipocyte-selective genes in differentiated cultures (Figure 2A,D). Importantly, *Zfp423* mRNA was almost entirely absent from these cultures, reflecting the activity of the *Wt1-Cre* line in this depot. Cultures of gonadal white adipocytes lacking *Zfp423* robustly activate their thermogenic gene program upon stimulation with forskolin (Figure 2E). These changes were accompanied by increased basal, uncoupled (oligomycin), and maximal (FCCP) respiration in differentiated gonadal adipocyte cultures from mutant animals (Figure 2F,G). These data indicate that *Zfp423*-deficient visceral adipose precursors can differentiate into functional thermogenic adipocytes in a cell-autonomous manner. The cellular phenotype of *Zfp423*-deficient visceral adipocytes is reminiscent of the characterized phenotype of subcutaneous beige adipocyte cultures (Wu et al., 2012); therefore, we examined whether *Zfp423*-deficient visceral adipocyte cultures are enriched in the expression of beige-selective transcripts. *Zfp423*-deficient visceral adipocytes expressed lower levels of white adipocyte-selective genes; however, we did not observe a clear pattern of gene expression changes that would indicate a conversion of *Zfp423*-deficient visceral adipocytes to either subcutaneous beige or classic brown fat cells (Figure 2H).

**Thermogenic *Zfp423*-deficient visceral adipose tissue is largely distinct from subcutaneous beige adipose tissue.**

Prior studies of the beige adipocyte determination factor, *Prdm16*, revealed that genetic ablation of *Prdm16* in adipose tissue leads to the loss of subcutaneous beige adipocytes, with inguinal WAT acquiring the molecular properties of visceral fat. Thus, we next asked whether the loss of *Zfp423* reprograms visceral WAT into subcutaneous WAT. Alternatively, visceral WAT lacking *Zfp423* may retain a global visceral phenotype but adopt a thermogenic phenotype reminiscent of classical brown or subcutaneous beige adipose tissues. In order to address this question we obtained and compared global gene expression profiles of adipose depots from control and Vis-KO animals through RNA sequencing (RNA-seq). For this experiment, we treated all animals with a  $\beta$ -3 adrenergic receptor agonist (CL316,243), or vehicle, for 3 days at thermoneutrality. This treatment allowed us to capture the global gene expression profile of thermogenic adipose depots in their fully active state. CL316,243 treatment led to a much greater increase in mRNA levels of *Ucp1* and most other thermogenic genes examined in visceral WAT depots of Vis-KO mice than in control animals (Figure 3A,B). Levels of *Ucp1* mRNA in the visceral depots lacking *Zfp423* nearly reached levels of *Ucp1* found in inguinal WAT following CL316,243 treatment (i.e. subcutaneous beige adipose tissue) (Figure 3A). This was accompanied by the widespread appearance of multilocular cells in gonadal WAT with readily detectable *Ucp1* protein expression (Figure 3C-F). We again assayed the mRNA levels of genes commonly used as white, beige, and classic brown, adipocyte markers. Similar to results obtained from cultured *Zfp423*-deficient visceral adipocytes, the expression of some white adipocyte-selective genes examined were lower in Vis-KO gWAT; however, we once again did not observe

a clear pattern of gene expression changes that would indicate a conversion of *Zfp423*-deficient gWAT to either subcutaneous beige or classic brown adipose tissue (Figure 3G).

Principal component analysis and unsupervised hierarchical clustering analysis of RNA-Seq data suggest that the global gene expression profile of *Zfp423*-deficient gWAT is distinct from subcutaneous beige adipose tissue and classic BAT. Instead, the *Zfp423*-deficient visceral WAT more closely resembles gWAT from control animals (Figure 4A-B). We next compared the list of transcripts that are differentially expressed between  $\beta$ 3-agonist treated *Zfp423*-deficient gWAT and  $\beta$ 3-agonist treated gWAT of control animals (i.e. genes whose expression reflect engineered thermogenic gWAT, Figure 4- source data 1) to the list of transcripts that are differentially regulated between  $\beta$ -agonist treated iWAT and vehicle-treated iWAT of control animals (i.e. genes whose expression reflects beige inguinal adipose tissue, Figure 4- source data 2). *Zfp423*-deficiency led to the differential expression of 1,735 transcripts in gWAT ( $\text{FDR} \leq 0.05$ ) (Figure 4C). Of these 1,735 transcripts, 207 genes (12%) overlap with genes differentially regulated following  $\beta$ 3-agonist treatment of iWAT (Figure 4- source data 3). Functional classification of these 207 genes by gene ontology analysis indicated that nearly all of these genes are related to mitochondrial function and biogenesis, a hallmark of thermogenic adipocytes (Figure 4D,E). These data suggest that *Zfp423*-deficient adipocytes present in Vis-KO animals are visceral adipocytes expressing at least a portion of the thermogenic gene program characteristic of subcutaneous beige adipocytes.



## **Thermogenic visceral adipose tissue confers improved cold tolerance and protection from insulin resistance in obesity**

Subcutaneous beige adipocytes exert beneficial effects on nutrient homeostasis and can increase energy expenditure. The Vis-KO model affords the opportunity to explore the systemic benefits of unlocking the thermogenic phenotype of visceral adipose depots. To this end, we tested the ability of Vis-KO mice to maintain body temperature in response to cold challenge. Following 1 week of cold exposure, visceral WAT depots of the Vis-KO mice activated their thermogenic gene program (Figure 5A,B) and accumulated Ucp1<sup>+</sup> multilocular adipocytes (Figure 5C-J) to a much greater extent than control animals. We did not observe a significant difference in core body temperature during an acute cold tolerance test of control and Vis-KO animals (Figure 5K); however, after four weeks of cold acclimation, the Vis-KO mice maintain higher core body temperature (Figure 5L). Collectively, these data demonstrate that inactivation of *Zfp423* is sufficient to unlock the thermogenic activity of visceral WAT depots under postnatal physiological conditions, and that browning of these depots can functionally enhance adaptive thermogenesis.

We also asked whether the thermogenic visceral WAT present in Vis-KO animals confers protection against diet-induced obesity and/or impaired nutrient homeostasis. We administered 8 weeks-old male mice chow or high-fat diet (HFD) (60% calories from fat) for 20 weeks. Over this period, we did not observe a significant difference in body weight between Vis-KO mice and controls (Figure 6A). At the time of analysis (8 weeks of HFD feeding), we did not observe a significant difference in adiposity (% body fat), lean mass, or fat distribution (Figure 6B,C). Gene expression analysis of dissected tissues revealed that the loss of *Zfp423* expression remained restricted to visceral

depots (Figure 6D). Levels of *Ucp1* and other genes related to thermogenesis were significantly increased in visceral depots of obese Vis-KO mice (Figure 6E,F); however, mRNA levels of adipocyte-selective genes did not appear to be impacted by the loss of *Zfp423* (Figure 6G). The latter suggests that *Zfp423*-deficiency did not impact de novo visceral adipocyte differentiation that occurs over this period of HFD feeding. The increase in thermogenic gene expression appeared functionally significant; rates of basal and maximal oxygen consumption were significantly elevated in the visceral depots of obese Vis-KO mice when compared to controls (Figure 6H-J). We again observed a slight increase in the expression of thermogenic genes in the inguinal WAT of mutant animals; however, the metabolic activity of the inguinal WAT depot did not significantly differ from inguinal WAT of obese control mice (Figure 6K).

We also examined whether the observed increase in visceral WAT oxygen consumption impacts whole-body levels of energy expenditure. We assessed energy expenditure and food intake in control and knockout animals fed HFD for 8 weeks. At this point, body weights and body composition were comparable between the two groups of animals (Figure 7A,B); however, we observed a modest, but statistically significant, increase in O<sub>2</sub> consumption, heat production, and CO<sub>2</sub> production, in the *Zfp423*-deficient mice (Figure 7C-F). We observed a slight increase in food intake over the dark cycle; however, these differences did not reach statistical significance (Figure 7G). Moreover, overall locomotor activity measurements and respiratory exchange ratios were similar between control and knockout animals (Figure 7H,I). These new data indicate that visceral WAT deletion of *Zfp423*, and subsequent visceral browning,

enhances energy expenditure, albeit not a strong enough degree to drive a robust difference in body weight.

Further metabolic phenotyping of control and mutant animals revealed that the beige-like phenotype of visceral WAT in diet-induced obese Vis-KO mice was associated with striking improvements in nutrient homeostasis. Obese Vis-KO mice exhibited significantly better glucose tolerance test than obese control animals; excursions in blood glucose and serum insulin following glucose challenge were substantially lower in Vis-KO animals (Figure 8A,B). Insulin tolerance tests suggest greater systemic insulin sensitivity in the Vis-KO mice (Figure 8C). We further explored the impact of visceral WAT browning on systemic glucose metabolism by performing hypersulinemic-euglycemic clamp assays. The glucose infusion rate needed to maintain euglycemia (~138 mg/dl) was increased in Vis-KO mice (Figure 8D). This demonstrates an increase in whole-body insulin sensitivity, consistent with the aforementioned insulin tolerance tests. Importantly, endogenous glucose output was suppressed much more efficiently during the basal and clamped states in Vis-KO mice, likely reflecting improved insulin sensitivity at the level of the liver (Figure 8E). These data are supported by liver gene expression analysis from a separate cohort of animals. The mRNA levels of key gluconeogenic genes in the Vis-KO livers are significantly lower than corresponding levels in livers from control animals after 8 weeks of HFD feeding (Figure 8F). Furthermore, visceral adipose-selective browning phenotype is associated with lower serum triglyceride levels (Figure 8G). <sup>14</sup>C-2-deoxyglucose tracing revealed that the rate of whole-body glucose disposal did not significantly differ between control and Vis-KO mice (Figure 8H); however, glucose uptake was enhanced in the visceral rWAT depot,

correlating with where the largest degree of visceral beiging is observed in this model (Figure 8I). All together, these data demonstrate visceral deletion of *Zfp423* leads to enhanced insulin sensitivity and reduced hepatic glucose output. Moreover, these data suggest that engineered thermogenic visceral adipose tissue, much like subcutaneous beige adipose tissue, can defend against the development of impaired glucose and lipid homeostasis in obesity.

**Inactivation of *Zfp423* in adult mural cells leads to beige, rather than white, adipocyte hyperplasia in diet-induced obesity.**

We previously demonstrated that adipocytes emerging in expanding visceral, but not subcutaneous, WAT depots of diet-induced obese mice arise through *de novo* adipocyte differentiation from mural progenitors expressing *Pdgfrb* (Hepler et al., 2017; Vishvanath et al., 2016). Whether these preadipocytes can be redirected to a thermogenic adipocyte fate, thereby driving beige-like adipocyte hyperplasia rather than white adipocyte hyperplasia, has been unclear. To address this, we generated a model that allows for doxycycline-inducible inactivation of *Zfp423* in *Pdgfrb*-expressing mural cells (inducible mural cell *Zfp423* knockout, or “iMural-KO”) (Figure 9A). The iMural-KO model was achieved by breeding *Pdgfrb*<sup>rtTA</sup> transgenic mice to animals expressing Cre recombinase under the control of a tetracycline responsive element (*TRE-Cre*) and carrying floxed *Zfp423* alleles (*Zfp423*<sup>loxP/loxP</sup>). We also bred the Cre-dependent Rosa26R *loxP*-mtdTomato-*loxP*-mGFP (mT/mG) fluorescent reporter allele into the model; this allowed for the fate-mapping of targeted mural cells. Treatment of adult animals with doxycycline leads to Cre dependent inactivation of mural cell *Zfp423* (Figure 9B), and permanent fluorescent-tagging (mGFP) of *Pdgfrb*<sup>+</sup> cells. Importantly,

mature adipocytes present at the time of doxycycline treatment are not targeted (Figure 9B). Only those adipocytes that descend from mural cells following HFD feeding are *Zfp423*-deficient and will express mGFP.

Following doxycycline treatment, we fed control and iMural-KO mice a HFD for 8 weeks (Figure 9C). After 8 weeks of HFD feeding, the body weights of mutant animals were indistinguishable from controls (Figure 9D). *De novo* white adipocyte differentiation occurred in gWAT of both control and mutant animals; newly derived adipocytes were indicated by the expression of mGFP (Figure 9E-J). However, we did not observe a statistically significant difference in the number of mGFP+ adipocytes between control and iMural-KO mice (Figure 9K). Overall, ~5-15% of gonadal adipocytes present in the gWAT of these obese animals descended from mural cells. Despite the fact that *Zfp423* expression identifies mural adipose progenitors, these data suggest that adult mural progenitors do not require *Zfp423* in vivo for their ability to undergo adipocyte differentiation in response to HFD feeding.

*Zfp423*-deficient adipocytes originating from mural progenitors in the obese iMural-KO model were readily identified by mGFP expression; however, these cells were not multilocular (Figure 9H,I,J). Moreover, the glucose tolerance of obese iMural-KO mice was similar to that of control animals (Figure 9L). Our previous study revealed that the thermogenic activity of *Zfp423*-deficient adipocytes was dependent on active  $\beta$ -adrenergic signaling (Shao et al., 2016); it is well appreciated that rodent obesity is associated with augmented  $\beta$ -adrenergic receptor signaling (Collins et al., 1999; Collins and Surwit, 2001). Therefore, we reasoned that the *Zfp423*-deficient adipocytes present in these obese mice would require a stimulus to fully activate their

thermogenic function in this setting. To test this, we utilized osmotic pumps to deliver the  $\beta$ 3-adrenergic receptor agonist, CL316,243, daily at a dose of 1mg/kg/day for four continuous weeks. The agonist was given to obese control and iMural-KO mice after 8 weeks of HFD feeding (Figure. 10A). During the 4 weeks of the  $\beta$ 3-agonist treatment, both control and iMural-KO animals exhibited a similarly mild decrease in body weight (Figure 10B). However, after four weeks of  $\beta$ 3-agonist treatment, the gonadal adipose depot mass of iMural-KO mice was significantly smaller than the gWAT mass of treated control mice (Figure 10C). Immunohistochemistry for mGFP expression revealed that  $\beta$ 3-agonist treatment did not induce the formation of any additional gonadal or inguinal adipocytes from the *Pdgfrb* lineage (Figure 10D-H, Figure 10 S1A,B). We again did not observe a difference in the numbers of mGFP-labelled adipocytes between control and knockout animals (Figure 10 S1A,B). Mural-cell derived adipocytes in the  $\beta$ 3-agonist treated control animals remained unilocular; however, most mGFP+ adipocytes present in  $\beta$ 3-agonist treated knockout mice were now multilocular (Figure 10D-H). On average, ~6% of gonadal adipocytes appeared multilocular in the iMural-KO animals; very few, if any, gonadal multilocular adipocytes were present in  $\beta$ 3-agonist treated control mice (Figure 10 S1C). Levels of *Ucp1* mRNA were strongly elevated in visceral depots of the  $\beta$ 3-agonist treated iMural-KO mice (Figure 10 S1E). On the other hand, the percentage of inguinal adipocytes appearing multilocular appeared low (~3%) and comparable between control and knockout animals (Figure 10 S1D). However, despite the low and comparable levels of mural cell adipogenesis, the iWAT from  $\beta$ 3-agonist treated knockout animals had relatively higher levels of *Ucp1* mRNA in comparison to controls (Figure 10 S1E). The recruitment of this relatively low number of beige-like adipocytes

394 appeared sufficient to drive an increase in basal respiration of adipose tissues (Figure  
395 10 S1F). This active thermogenic phenotype of the visceral WAT correlated with  
396 markedly improved glucose tolerance and insulin sensitivity observed in  $\beta$ 3-agonist  
397 iMural-KO mice (Figure 10I-K). All together, these data indicate that visceral mural  
398 preadipocytes in adult mice can be directed to a dormant beige-like phenotype in the  
399 expanding visceral WAT depots of diet-induced obese animals. Upon activation by  $\beta$ 3  
400 adrenergic receptor agonism, these beige-like adipocytes appear to drive an  
401 improvement in insulin sensitivity in obese animals.

## Discussion

It is now certain that adult humans have appreciable amounts of thermogenic adipose tissue consisting of brown and beige adipocytes (Cypess et al., 2013; Shinoda et al., 2015; van Marken Lichtenbelt et al., 2009; Virtanen et al., 2009). Upon activation, thermogenic adipose tissue in lean adults can impact glucose and lipid homeostasis (Chondronikola et al., 2014; Chondronikola et al., 2016; Cypess et al., 2015); however, it still remains unclear as to whether sufficient amounts of thermogenic adipose tissue are present in obese individuals to exert beneficial therapeutic effects, even when fully activated. As such, there is tremendous interest in identifying strategies to increase the mass of functional thermogenic adipose tissue in obese patients with metabolic syndrome. To this end, a number of studies have now identified pathways/factors that can drive the natural formation of subcutaneous beige adipocytes or classic brown adipocytes (Harms and Seale, 2013). The negative impacts of visceral expansion during obesity on metabolic health make visceral fat a prime target for therapeutic intervention; however, effective strategies to improve the health of visceral WAT health have yet to emerge. In particular, whether browning of visceral depots, much like the browning of subcutaneous adipose tissue, would exert beneficial metabolic effects has been unclear.

We recently reported that *Zfp423* is a suppressor of the thermogenic gene program in adipocytes. Using this discovery as a tool, we reveal here that the thermogenic potential of visceral adipose depots in mice can be unlocked through removal of *Zfp423*. Importantly, these data provide proof of concept that white adipose precursors in adult animals can be redirected to a beige-like adipocyte fate and improve



insulin sensitivity in obesity. Overall, we observed beneficial effects of visceral WAT browning on nutrient homeostasis and cold tolerance. Nevertheless, we cannot exclude the possibility that inducing the thermogenic capacity of these depots may have detrimental effects under other physiological conditions not examined. Elevated expression of *Zfp423* in visceral white adipocytes provides one explanation as to how visceral WAT depots resist adopting a thermogenic phenotype; however, it remains unclear as to why visceral WAT depots would adopt these anti-thermogenic mechanisms.

Inactivation of *Zfp423* in visceral WAT gives rise to thermogenic adipocytes that share properties of subcutaneous beige adipocytes and classic brown adipocytes. In particular, *Zfp423* deletion in visceral WAT unlocks a functionally significant portion of the thermogenic gene program characteristic of activated ( $\beta$ 3 adrenergic receptor activated) beige adipose tissue. Nevertheless, global gene expression profiling suggests that *Zfp423*-deficient visceral WAT largely retains a visceral WAT molecular signature, rather than adopting the global molecular program characteristic of subcutaneous WAT. Additional gene expression studies of isolated visceral and inguinal Ucp1+ adipocytes will be needed to fully characterize the similarities and differences between the anatomically distinct thermogenic fat cells. During preparation of this manuscript, Kirichok and colleagues reported the existence of two distinct types of thermogenic beige adipocytes present in visceral depots of mice stimulated with the  $\beta$ 3-adrenergic receptor agonist for 10 days (Bertholet et al., 2017). In particular, Bertholet et al. revealed that most thermogenic adipocytes in visceral WAT are devoid of Ucp1 protein and instead employ futile creatine cycling for thermogenesis. *Zfp423*-deficient

visceral adipocytes express Ucp1 protein; however, the precise contribution of Ucp1-mediated uncoupling vs. creatine cycling in these cells remains unclear.

Our data here highlight the ability of thermogenic adipocytes, even within the visceral compartment, to drive vast improvements in nutrient homeostasis in obese mice, without impacting body weight. Moreover, the mural cell knockout model of *Zfp423* even suggests that a relatively low frequency of activated multilocular *Zfp423*-deficient visceral adipocytes (5-10% of adipocytes in  $\beta$ 3-agonist treated obese iMural-KO mice) can lead to improved insulin sensitivity. This is surprising given the opinion that such small numbers of beige cells are not likely to confer significant benefit (Kalinovich et al., 2017). We, of course, cannot rule out the possibility that *Zfp423* deficiency may impact the visceral adipose phenotype in a multitude of ways that influence energy metabolism. It is notable that in the Vis-KO model, the data largely point to the liver as a major site of improved insulin sensitivity. Previously reported work on *Prdm16* and subcutaneous WAT beiging suggest a strong connection between subcutaneous beige cells and liver health (Cohen et al., 2014). For the field at large, it remains an open question as to how brown/beige adipocytes exert beneficial effects on systemic metabolism, independent of their impact on body weight. This unique model may serve as a tool to explore the mechanisms of how visceral WAT browning leads to improved glucose metabolism.

We consistently observed a modest, yet statistically significant, induction of the thermogenic gene program in the inguinal WAT depots of both genetic models. There is a limit to our ability to interpret these results from the iMural-KO mice. Inguinal adipocyte differentiation is not impacted in this model; however, *Zfp423* is still

471 inactivated in mural cells of this depot. It is not possible to exclude additional roles for  
472 *Zfp423* in mural cells of iWAT or other tissues. Nevertheless, the dependency of the  
473 improved insulin sensitivity in obese iMural-KO mice on  $\beta$ 3-adrenergic receptor  
474 activation does suggest that the increased numbers of thermogenic visceral adipocytes,  
475 at least in part, contribute to the phenotypes observed here. In the Vis-KO model,  
476 inactivation of *Zfp423* is limited to visceral WAT depots. The subcutaneous WAT  
477 phenotype in this model is thus not cell autonomous and appears secondary to the  
478 visceral phenotype. It is possible that *Zfp423*-deficient visceral adipocytes produce  
479 circulating adipokines that influence systemic metabolism and thermogenesis. In fact,  
480 more and more “Batokines” have recently emerged (Lynes et al., 2017; Svensson et al.,  
481 2016; Thomou et al., 2017; Villarroja et al., 2017). It is also possible that secondary  
482 browning of subcutaneous WAT may be triggered through central effects mediated by a  
483 visceral WAT to brain neural relay.

484 A multitude of studies now support the idea that visceral adipocytes are  
485 developmentally, molecularly, and functionally, distinct from subcutaneous adipocytes.  
486 Our prior work revealed a critical role for *Zfp423* in 3T3-L1 adipogenesis and in the  
487 regulation of *Pparg* and the fetal formation of subcutaneous white adipocytes in vivo  
488 (Gupta et al., 2010; Shao et al., 2017). Our work here reveals that *Zfp423* is  
489 dispensable for the differentiation of visceral adipocytes within those visceral depots  
490 examined. Thus, *Zfp423* expression defines mural white preadipocytes within visceral  
491 depots of adult mice; however, other factors can compensate for its absence in the  
492 initial stages of adipocyte differentiation, but not in suppressing the thermogenic gene  
493 program. The lack of impact on adipocyte differentiation was unexpected; however, this

result is perhaps not surprising in light of recent studies of another pro-adipogenic transcription factor, *Cebpa*. In vitro, *Cebpa* is amongst the most critical adipogenesis factors; however, in vivo, it appears essential for postnatal, but not fetal, terminal differentiation of fat cells (Wang et al., 2015). Thus, despite the expression of *Cebpa* throughout the adipose lineage, there appears to be temporal requirements for this particular factor. These data, along with other studies, highlight the emerging concept that distinct transcriptional regulatory mechanisms govern fetal vs. adult adipogenesis (Jeffery et al., 2015; Wang et al., 2015). Our data here further highlight the complexity in the regulation of adipogenesis *in vivo* by demonstrating the depot-specific requirements of pro-adipogenic transcription factors.

*Zfp423* expression in the adipose lineage appears highly regulated. Levels of *Zfp423* in white adipocytes are reduced following cold exposure and  $\beta$ -adrenergic receptor agonism, and increased in brown adipose depots undergoing a “whitening” transformation with age or in obesity (Shao et al., 2016). The dynamic expression of *Zfp423*, along with the loss of function data from our genetic mouse models, reveal *Zfp423* as a critical physiological suppressor of the adipocyte thermogenic gene program. Future studies into the regulation of *Zfp423* expression in adipocytes and/or mural adipose precursors may lead to novel strategies to unlock the thermogenic potential of visceral adipose tissue and combat the chronic metabolic defects associated with visceral obesity.

## Acknowledgements

The authors are grateful to members of the UTSW Touchstone Diabetes Center for useful discussions, and Drs. P. Scherer, and C. Kusminski for critical reading of the manuscript. The authors thank the UTSW Animal Resource Center, McDermott Sequencing Center, Metabolic Phenotyping Core, Pathology Core, Live Cell Imaging Core, and Flow Cytometry Core for excellent guidance and assistance with experiments performed here. This study was supported by the Searle Scholars Program (Chicago, IL) and NIDDK R01 DK104789 to R.K.G., NIDDK R00-DK094973 and JDRF Award 5-CDA-2014-185-A-N to W.L.H., F30 DK100095 to J.Y.X., the American Heart Association postdoctoral fellowship, 16POST26420136, to M.S, F31 DK113696-01 and NIH NIGMS T32 GM008203, to C.H.

## Materials and Methods

**Animals.** All animal experiments were performed according to procedures approved by the UTSW Animal Care and Use Committee. *Pdgfrb*<sup>rtTA</sup> transgenic mice (C57BL/6-Tg(Pdgfrb-rtTA)58Gpt/J; JAX 028570; RRID:IMSR\_JAX:028570) were previously described (Vishvanath et al., 2016). *TRE-Cre* (B6.Cg-Tg(tetO-cre)1Jaw/J; JAX 006234; RRID:IMSR\_JAX:006234), *Rosa26R*<sup>mT/mG</sup> (B6.129(Cg)-*Gt(ROSA)26Sor*<sup>tm4(ACTB-tdTomato,-EGFP)Luo</sup>/J; JAX 007676; RRID:IMSR\_JAX:007676), and *WT1-Cre* (*Wt1*<sup>tm1(EGFP/cre)Wtp</sup>/J; JAX 010911; RRID:IMSR\_JAX:010911) mice were obtained from Jackson Laboratories. *Zfp423*<sup>loxP/loxP</sup> mice were a gift from Dr. S. Warming (Genentech) (Warming et al., 2006). Mice were maintained on a 12 hr light/dark cycle in a temperature-controlled environment (room temperature, 22°C; thermoneutrality, 30°C; cold exposure, 6°C). Mice were given free access to food and water, and maintained on a standard chow diet, Dox-containing chow (600 mg/kg doxycycline, Bio-Serv, S4107), or a dox-containing HFD (600 mg/kg dox, 60% kcal% fat, BioServ, S5867). For acute  $\beta$ -3 adrenergic agonist administration, mice were transferred to 30°C chambers for two weeks then injected intraperitoneally with vehicle or CL316243 (1mg/kg/day) for 3 days. For chronic  $\beta$ -3 adrenergic agonist administration, mice were anesthetized by 2% isoflurane, and Alzet osmotic minipumps filled with vehicle (PBS) or CL 316243 (1mg/kg/24hr) were implanted subcutaneously in the dorsal region of the animals.

**Histological analysis.** Adipose tissues were harvested from perfused (4% paraformaldehyde) adult mice. Paraffin processing and embedding was performed by the Molecular Pathology Core Facility at UTSW. Indirect immunofluorescence was performed as previously described (Vishvanath et al., 2016). Antibodies used for

immunofluorescence include: anti-GFP 1:700 (Abcam ab13970, RRID:AB\_300798), anti-perilipin 1:1500 (Fitzgerald 20R-PP004, RRID:AB\_1288416), anti-chicken Alexa 488 1:200 (Invitrogen, RRID:AB\_142924), anti-guinea pig Alexa 647 1:200 (Invitrogen, RRID:AB\_141882), and anti-guinea pig Alexa 488 1:200 (Invitrogen, RRID:AB\_142018). For Ucp1 immunohistochemistry, paraffin-embedded sections were incubated with anti-Ucp1 (Abcam ab10983; 1:500, RRID:AB\_2241462), followed by secondary and tertiary signal amplification and detection using biotinylated anti-rabbit secondary (Vector BA-1100, RRID:AB\_2336201), HRP-conjugated streptavidin (Dako), and DAB substrate (Thermo). For quantification of adipocyte hyperplasia, paraffin sections were stained with perilipin and GFP by indirect immunofluorescence. The number of GFP+ perilipin+ and GFP- perilipin+ adipocytes were counted on 8-10 randomly selected 10X images of stained WAT depots. A total of 3,000-5,000 perilipin+ adipocytes were counted from each mouse. Each data point represents the percentage of GFP+ perilipin+ adipocytes from one mouse.

**Isolation of adipose tissue SVF and FACS.** SVF was isolated as previously described (Shao et al., 2016). Briefly, minced adipose tissue was placed in digestion buffer (100mM HEPES pH 7.4, 120 mM NaCl, 50 mM KCl, 5 mM glucose, 1 mM CaCl<sub>2</sub>, 1.5% BSA, and 1mg/mL collagenase D (Roche 11088882001) and incubated in a 37°C shaking water bath for 2 hours. The mixture was then passed sequentially through a 100 µm cell strainer then a 40 µm cell strainer. Cells were blocked in 2% FBS/PBS containing anti-mouse CD16/CD32 Fc Block (clone 2.4G2; 1:200; RRID:AB\_394657), then incubated with primary antibodies (anti-CD31 clone 390 1:200, RRID:AB\_312903; anti-CD45 clone 30-F11 1:200, RRID:AB\_312971; anti-CD140b clone APB5 3:200,

574 RRID:AB\_2268091). Cells were sorted using a FACS Aria™ flow cytometer (UTSW Flow  
575 Cytometry Core Facility).

576 **Adipocyte differentiation assays.** Adipose tissue SVF was isolated as described  
577 above. Cells were plated onto collagen-coated dishes and incubated at 10% CO<sub>2</sub>.  
578 Gonadal SVF was maintained in growth media (60% pH7–7.4 low glucose DMEM, 40%  
579 pH 7.25 MCDB201 (Sigma M6770)), supplemented with 2% FBS (Fisher Scientific 03-  
580 600-511 Lot FB-002) 1% ITS premix (Insulin-Transferrin-Selenium) (BD Bioscience  
581 354352), 0.1 mM L-ascorbic acid-2-phosphate (Sigma A8960-5G), 10ng/mL FGF basic  
582 (R&D systems 3139-FB-025/CF), Pen/Strep, and gentamicin. Inguinal SVF was  
583 maintained in DMEM/F12 (Invitrogen) supplemented with Glutamax, 10% FBS,  
584 Pen/Strep, and gentamicin. Upon reaching confluence, cultures were incubated with the  
585 adipogenesis induction cocktail (growth media supplemented with 5 mg/ml insulin, 1 μM  
586 dexamethasone, 0.5 mM isobutylmethoxyxanthine, and 1 μM rosiglitazone) for 48 hr. After  
587 48 hr, the cells were maintained in growth media supplemented with 5 mg/ml insulin and  
588 1 μM rosiglitazone until harvest.

589 **Oil red O staining.** Differentiated cells were fixed in 4% PFA for 15 min at room  
590 temperature then washed twice with water. Cells were incubated in Oil Red O working  
591 solution (2 g Oil red O in 60% isopropanol) for 10 min to stain accumulated lipids. Cells  
592 were then washed three times with water before bright field images were acquired.

593 **Gene expression analysis.** Relative mRNA levels were determined by quantitative  
594 PCR using SYBR Green chemistry. Values were normalized to Rps18 levels using the  
595  $\Delta\Delta$ -Ct method. Unpaired Student's t-test was used to evaluate statistical significance.



All primer sequences are listed in Table 1. mRNA library preparation and RNA-sequencing was performed by the McDermott Center Sequencing Core at UT Southwestern. Total RNA used for library preparation was extracted from gonadal, inguinal, and brown adipose tissues of Control and Vis-KO mice after 3 days of treatment with CL-316,243 at thermoneutrality, as described above. Sequencing was performed on an Illumina HiSeq 2500 and reads were mapped to the mouse genome (mm10). Analysis was performed by the UT Southwestern McDermott Bioinformatics Core using Cufflinks/Cuffdiff software. Genes with an FDR < 0.05 were considered significantly differentially expressed between groups compared. Heatmaps were generated using the Pheatmap package in RStudio (v3.3). The cluster dendrogram was generated using Hierarchical Cluster Analysis in RStudio (v3.3). Gene Ontology analysis was performed using the DAVID Functional Annotation tool (<https://david.ncifcrf.gov/>) on differentially expressed genes between groups compared. Functional annotation for gene ontology using the GOTERM\_CC\_FAT category was selected and biological processes were assessed for statistical significance. All raw sequencing data has been deposited to Gene Expression Omnibus (<https://www.ncbi.nlm.nih.gov/geo/query/acc.cgi?acc=GSE98132>).

**Metabolic phenotyping.** Metabolic cage studies were conducted using TSE Phenomaster cages (TSE Systems, Chesterfield, Missouri) at the USTW Metabolic Phenotyping Core. Mice were acclimated in the metabolic chambers for 5 days before the start of the experiments. Food intake, movement, and CO<sub>2</sub> and O<sub>2</sub> levels were measured every 60 min for each mouse over a period of 5 days. For glucose tolerance tests, mice were fasted overnight and then administered glucose by intraperitoneal

619 injection (1 g/kg body weight, Sigma). For insulin tolerance tests, mice were fasted for 4  
620 hours and then administered insulin by intraperitoneal injection (0.75 U/kg body weight  
621 human insulin, Eli Lilly). At the indicated time-points, tail blood was collected.  
622 Hyperinsulinemic euglycemic clamps were performed on conscious, unrestrained mice  
623 as previously described (Holland et al., 2011). Blood glucose was measured using  
624 Bayer Contour glucometers. Serum triglycerides were measured using Infinity  
625 Triglycerides Reagent (Thermo Fisher Scientific). Serum insulin was measured using  
626 Ultra Sensitive Mouse Insulin ELISA (Crystal Chem).

627 **Cold Exposure.** Mice 8 weeks of age were transferred to a 30°C chamber  
628 (thermoneutrality) for two weeks. One week before cold exposure, IPTT-300  
629 temperature transponders (Bio Medic Data Systems) were implanted subcutaneously in  
630 the in the dorsal region of the mice. Body temperature was assessed using a DAS-  
631 7006/7s reader (Bio Medic Data Systems). The mice were then transferred to the cold  
632 chamber (6°C) or maintained at thermoneutrality. For the acute cold tolerance test, food  
633 was removed from the cages upon transfer to the cold chamber and body temperature  
634 was measured at the indicated time points. For the acclimated cold exposure test, food  
635 was removed from the cages after 4 weeks of acclimation to cold and body temperature  
636 was measured at the indicated time points.

637 **Mitochondrial function and respiration.** Adipose tissue fragments or cultured  
638 adipocytes were assayed for oxygen consumption rate (OCR) using an XF24  
639 Extracellular Flux Analyzer (Seahorse Bioscience, MA). Assays of mitochondrial  
640 function and respiration rates in whole adipose tissues or cells were performed as  
641 previously described (Shao et al., 2016). In brief, adipose tissue was cut into 5-10 mg

pieces and locked into an XF24 islet-capture Microplate (Seahorse Bioscience). Adipose tissues or cultured adipocytes were equilibrated for 1 h at 37°C in a CO<sub>2</sub>-free incubator in XF Assay Medium (Modified DMEM, 0 mM Glucose; Seahorse Bioscience) (pH 7.4), supplemented with 1mM sodium pyruvate, 1 mM L- Glutamine and 7 mM glucose. Tissues or cells were subjected to a 10-min equilibration period and 3 assay cycles to measure the basal rate, comprising a 3-min mix, a 2-min wait and a 3- min measure period each. For cells, compounds were then added by automatic pneumatic injection followed by assay cycles after each, comprising of 3-min mix, 2-min wait and a 3-min measure period. OCR measurements were obtained following sequential additions of oligomycin (3 µM final concentration), FCCP (9 µM) and antimycinA/rotenone (3 µM/30 nM). OCR measurements were recorded at set interval time points. All compounds and materials above were obtained from Sigma-Aldrich.

**Statistical Analysis.** All data were expressed as the mean ± SEM. We used GraphPad Prism 7.0 (GraphPad Software, Inc., La Jolla, CA, USA) to perform the statistical analyses. Each experiment was performed at least twice and representative data are shown. For comparisons between two independent groups, a Student's *t*-test was used and *p*<0.05 was considered statistically significant. The sample size estimation was determined as described below. All the detailed sample sizes, statistical test methods, and *p*-values are listed in Table 2. Longitudinal metabolic cohorts were designed to detect a 25% improvement of glucose tolerance or a similar magnitude of insulin resistance with an assumed 15% standard deviation of the group means at a power of 80% and an alpha of 0.05. This predicted approximately 6 animals per test group. All animals in the cohort were subsequently used for downstream assays (gene

expression, IHC, western blot) to eliminate selection bias. We estimated the approximate effect size based on independent preliminary studies. Studies designed to characterize an *in vitro* difference in metabolic flux were estimated to have a slightly larger effect size of 30% with assumed 15% standard deviation of group means. To detect this difference at a power of 80% and an alpha of 0.05, we predicted we would need 4 independent replicates per group. We estimated this effect size based on independent preliminary studies.

## Figure Legends

### Figure 1. Deletion of *Zfp423* in fetal visceral white adipocyte precursors leads to the formation of thermogenic adipocytes in visceral depots.

(A) A mouse model of visceral WAT selective ablation of *Zfp423* (Visceral-Knockout or “Vis-KO”) was derived by breeding animals expressing the gene encoding Cre recombinase under the control of the *Wilms Tumor 1* (*WT1*) promoter to animals carrying floxed *Zfp423* alleles (*Zfp423*<sup>loxP/loxP</sup>). Littermates carrying only *Zfp423*<sup>loxP/loxP</sup> alleles were used as control animals.

(B) Fold change in mRNA levels within brown (BAT), inguinal (iWAT), gonadal (gWAT), mesenteric (mWAT), or retroperitoneal (rWAT) adipose tissue of control (white bar) and Vis-KO (red bar) mice at 8 weeks of age. \* denotes p<0.05 from unpaired Student’s t-test. n = 6 mice.

(C) Body weight of control (white bar) and Vis-KO (red bar) mice at 8 weeks of age. n = 6 mice.

(D) Fat pad weight (normalized to body weight) of control (white bar) and Vis-KO (red bar) mice at 8 weeks of age. \* denotes p<0.05 from unpaired Student’s t-test. n = 6 mice.

(E- F) Fold change in mRNA levels of mature adipocyte genes (E) and thermogenic genes (F) isolated from whole adipose tissue from control (white bar) and Vis-KO (red bar) mice at 8 weeks of age. \* denotes p<0.05 from unpaired Student’s t-test. n = 6 mice.

(G) mRNA levels (normalized to *Rps18*) of *Ucp1* isolated from whole adipose tissue from control (white bar) and Vis-KO (red bar) mice at 8 weeks of age. \* denotes p<0.05 from unpaired Student’s t-test. n = 6 mice.

(H-K) Relative basal oxygen consumption rates (OCRs) within diced gWAT (H), mWAT (I), rWAT (J), and iWAT (K) from control (white bar) and Vis-KO (red bar) mice at 8 weeks of age. \* denotes  $p < 0.05$  from unpaired Student's t-test.  $n = 4$  independent replicates pooled from 2 mice.

(L-O) Representative immunofluorescence staining of Perilipin (green) and DAPI (blue) in mWAT sections obtained from control (L, M) and Vis-KO (N, O) mice at 8 weeks of age. Scale bar, 200  $\mu$ M. Panels M and O represent digital enhancements of the boxed regions shown in L and N, respectively.

#### **Figure 1- Supplement 1**

(A-L) Representative images of gonadal (gWAT), retroperitoneal (rWAT), and inguinal WAT (iWAT) from control and Vis-KO mice immunostained with antibodies raised against Perilipin (green). Scale bar = 200  $\mu$ M. Panels B,D,F,H,J, and L represent digital enhancements of the boxed regions shown in A, C, E, G, I, and K, respectively.

**Figure 2. *Zfp423*-deficient visceral adipose precursors differentiate into functional thermogenic adipocytes *in vitro*.**

(A) Oil Red O staining of adipocytes differentiated *in vitro* from inguinal and gonadal SVF of control and Vis-KO mice.

(B) Fold change in mRNA levels of adipocyte-selective genes in inguinal adipocyte cultures differentiated as shown in A. \* denotes  $p < 0.05$  from unpaired Student's t-test.  $n = 4$  replicates from two mice.

(C) Fold change in mRNA levels of thermogenic genes in inguinal adipocyte cultures differentiated as shown in A and treated with vehicle or forskolin ( $10 \mu\text{M}$ ) for 3 hours.  $n = 4$  replicates from two mice.

(D) Fold change in mRNA levels of adipocyte-selective genes in gonadal adipocyte cultures as shown in A. \* denotes  $p < 0.05$  from unpaired Student's t-test.  $n = 4$  replicates from two mice.

(E) Fold change in mRNA levels of thermogenic genes in gonadal adipocyte cultures differentiated as shown in A and treated with vehicle or forskolin ( $10 \mu\text{M}$ ) for 3 hours. \* denotes  $p < 0.05$  from unpaired Student's t-test.  $n = 4$  replicates from two mice.

(F) Oxygen consumption rates (OCRs) within differentiated cultures of control (white bars) or *Zfp423*-deficient (red bars) gonadal adipocytes in the basal state, and in response to sequential additions of oligomycin (ATP synthase inhibitor), FCCP (chemical uncoupler), and rotenone/antimycin A (complex I and complex III inhibitor). \* denotes  $p < 0.05$  from unpaired Student's t-test.  $n = 4$  replicates from two mice.

(G) Percent uncoupled respiration of differentiated cultures of control (white bar) or *Zfp423*-deficient (red bar) gonadal adipocytes as determined by basal and uncoupled

739 (oligomycin) respiration data from Figure 2F. \* denotes  $p < 0.05$  from unpaired Student's  
740 t-test. n = 4 replicates from two mice.

741 (H) Fold change in mRNA levels of white-, beige-, and brown-selective genes in  
742 differentiated cultures of control (white bars) or *Zfp423*-deficient (red bars) gonadal  
743 adipocytes. \* denotes  $p < 0.05$  from unpaired Student's t-test. n = 4 replicates from two  
744 mice.

745

746

747

748



**Figure 3. Visceral adipose tissue deletion of *Zfp423* leads to enhanced visceral browning upon  $\beta$ -3 adrenergic receptor agonism at thermoneutrality.**

(A) Control and Vis-KO mice were housed at room temperature (22°C) until 6 weeks of age then transferred to thermoneutral housing conditions (30°C) for 2 weeks. After 2 weeks at thermoneutrality, mice were treated with PBS (vehicle) or CL316,243 (1 mg/kg, intraperitoneal) daily for 3 days. On the 4<sup>th</sup> day, tissues were harvested for analysis. mRNA levels (relative to *Rps18*) of *Ucp1* in iWAT, gWAT, and rWAT obtained from control and Vis-KO mice treated with vehicle or CL316,243 (CL) for 3 days at thermoneutrality. \* denotes  $p < 0.05$  from unpaired Student's t-test.  $n = 4-5$  mice.

(B) Fold change in mRNA levels of thermogenic genes in gWAT obtained from control and Vis-KO mice treated with vehicle or CL316,243 (CL) for 3 days at thermoneutrality. \* denotes  $p < 0.05$  from unpaired Student's t-test.  $n = 4-5$  mice.

(C-F) Representative brightfield images of *Ucp1* immunoreactivity (brown staining) in gWAT sections obtained from control or Vis-KO mice treated with vehicle (C,D) or CL316,243 (E,F).

(G) Fold change in mRNA levels of white-, beige-, and brown-selective genes in gWAT obtained from control and Vis-KO mice treated with vehicle or CL316,243 (CL) for 3 days at thermoneutrality. \* denotes  $p < 0.05$  from unpaired Student's t-test.  $n = 4-5$  mice.

**Figure 4. Thermogenic *Zfp423*-deficient visceral adipose tissue is largely distinct from subcutaneous beige adipose tissue.**

(A) RNA-sequencing was performed on mRNA libraries derived from gonadal WAT (gWAT) of vehicle- and  $\beta 3$  agonist (CL)-treated control and Vis-KO mice, as well as from inguinal WAT and interscapular BAT of vehicle- and CL-treated control mice. Principle component (PC) analysis of sequencing data obtained from CL-treated animals.  $n = 3$  sequenced libraries for each condition.

(B) Unsupervised clustering dendrogram of adipose depot samples.

(C) Venn diagram depicting overlap in 1) transcripts that are differentially expressed between  $\beta 3$ -agonist treated *Zfp423*-deficient gWAT and  $\beta 3$ -agonist treated gWAT of control animals, and 2) transcripts that are differentially regulated between  $\beta$ -agonist treated iWAT and vehicle-treated iWAT of wild-type animals. See Figure 4- source data 1, Figure 4- source data 2, Figure 4- source data 3.

(D) Gene ontology analysis (GOTERM\_CC\_FAT) of the 207 overlapping genes shown in C.

(E) Heatmap of top 50 induced genes of the 207 highlighted in C.

**Figure 5. *Zfp423*-deficiency enables cold-induced visceral WAT browning.**

(A) Control and Vis-KO mice were housed at room temperature (22°C) until 6 weeks of age then transferred to thermoneutral housing (30°C) for 2 weeks. After 2 weeks at thermoneutrality, animals were transferred to 6°C or left at thermoneutrality for 7 full days. On the 8<sup>th</sup> day, tissues were harvested for analysis. mRNA levels (relative to *Rps18*) of *Ucp1* in iWAT, gWAT, and rWAT from control and Vis-KO mice cold exposed (CE) or housed at thermoneutrality (TN) for 7 days. \* denotes p<0.05 from unpaired Student's t-test. n = 4-5 mice.

(B) Fold change in mRNA levels of thermogenic genes in rWAT and gWAT from control and Vis-KO mice cold exposed (CE) or housed at thermoneutrality (TN) for 7 days. \* denotes p<0.05 from unpaired Student's t-test. n = 4-5 mice.

(C-J) Brightfield images of *Ucp1* immunostaining (brown) within rWAT (C-F) and gWAT (G-J) sections obtained from control or Vis-KO mice following cold exposure (CE) or housing at thermoneutrality (TN).

(K) Body temperature at indicated time points following transfer of mice from thermoneutrality to cold (6°C). n = 4-5 mice

(L) Body temperature at indicated time points during a cold tolerance test after 4 weeks of acclimation to cold (6°C). \* denotes p<0.05 from unpaired Student's t-test. n = 4-5 mice.

**Figure 6. Obese mice lacking *Zfp423* in visceral adipose tissue display enhanced visceral adipose tissue thermogenesis.**

(A) Weekly measurements of body weights of 8 weeks-old control and Vis-KO mice fed a standard chow diet (Chow) or high fat diet (HFD) for 20 weeks. n = 6-7 mice per group.

(B) Total fat mass, lean mass, and water mass (normalized to body weight) of control (white bars) and Vis-KO (red bars) mice after 8 weeks of HFD feeding. n = 6-7 mice.

(C) Fat depot mass (normalized to body weight) of control (white bars) and Vis-KO (red bars) mice after 8 weeks of HFD feeding. n = 6-7 mice.

(D) Relative mRNA levels of *Zfp423* in BAT, iWAT, gWAT, mWAT, and rWAT isolated from control (white bars) and Vis-KO (red bars) mice after 8 weeks of HFD feeding. \* denotes  $p < 0.05$  from unpaired Student's t-test. n = 6-7 mice per group.

(E) mRNA levels (normalized to *Rps18*) of *Ucp1* within adipose depots of control (white bars) and Vis-KO (red bars) mice after 8 weeks of chow or HFD feeding. \* denotes  $p < 0.05$  from unpaired Student's t-test. n = 6-7 mice.

(F-G) Relative mRNA levels of thermogenic genes (F) and adipocyte-selective genes (G) in iWAT, gWAT, mWAT, and rWAT isolated from control (white bars) and Vis-KO (red bars) mice after 8 weeks of HFD feeding. \* denotes  $p < 0.05$  from unpaired Student's t-test. n = 6-7 mice.

(H-K) Relative basal oxygen consumption rates (OCRs) within gWAT (H), mWAT (I), rWAT (J), and iWAT (K) isolated from control (white bars) and Vis-KO (red bars) mice after 8 weeks of chow or HFD feeding. \* denotes  $p < 0.05$  from unpaired Student's t-test. n = 4 independent replicates pooled from 2 mice.

**Figure 7. Browning of visceral adipose tissues is associated with increased energy expenditure.**

(A) Body weight of control (white bar) and Vis-KO (red bar) mice after 8 weeks of high fat diet feeding. n = 4-5 mice.

(B) Total fat mass, lean mass, and water mass (normalized to body weight) of control (white bars) and Vis-KO (red bars) mice after 8 weeks of HFD feeding. n = 4-5 mice.

(C) O<sub>2</sub> consumption during two complete 12 hr light-dark cycles of control and Vis-KO mice following 8 weeks of high fat diet feeding. n = 4-5 mice.

(D-G) Average O<sub>2</sub> consumption (D), heat production (E), CO<sub>2</sub> production (F), and food intake (G) during the 24-hour, day, and night cycle in control (white bars) and Vis-KO (red bars) mice following 8 weeks of high fat diet. Bars represent averages from over the course of the 5-day measurement. \* denotes p<0.05 from unpaired Student's t-test. n = 4-5 mice.

(H) Average 24-hour X-beam, Y-beam, and Z-beam breaks of control (white bars) and Vis-KO (red bars) mice following 8 weeks of high fat diet. Bars represent averages from over the course of the 5-day measurement. n = 4-5 mice.

(I) Average RER during the 24-hour, day, and night cycle in control (white bars) and Vis-KO (red bars) mice following 8 weeks of high fat diet. Bars represent averages from over the course of the 5-day measurement. n = 4-5 mice.

**Figure 8. Mice lacking visceral adipose *Zfp423* are protected against insulin resistance in obesity.**

(A) Intraperitoneal glucose tolerance tests of control and Vis-KO mice after 8 weeks of chow or HFD feeding. \* denotes  $p < 0.05$  from unpaired Student's t-test.  $n = 6-7$  mice.

(B) Serum insulin levels of control and Vis-KO mice after 8 weeks of HFD feeding during the glucose tolerance test shown in A. \* denotes  $p < 0.05$  from unpaired Student's t-test.  $n = 6-7$  mice.

(C) Insulin tolerance tests of control and Vis-KO mice after 8 weeks of HFD feeding. \* denotes  $p < 0.05$  from unpaired Student's t-test.  $n = 6-7$  mice.

(D-E) Glucose infusion rate (D) and basal and clamped hepatic glucose production (E) during hyperinsulinemic-euglycemic clamp experiments performed on conscious, unrestrained control (white bars) and Vis-KO (red bars) mice after 8 weeks of HFD feeding. \* denotes  $p < 0.05$  from unpaired Student's t-test.  $n = 5-6$  mice.

(F) Relative mRNA levels of gluconeogenic genes in the livers of control (white bars) and Vis-KO (red bars) mice after 8 weeks of HFD feeding. \* denotes  $p < 0.05$  from unpaired Student's t-test.  $n = 6-7$  mice.

(G) Serum triglyceride levels in control (white bars) and Vis-KO (red bars) mice after 8 weeks of HFD feeding. \* denotes  $p < 0.05$  from unpaired Student's t-test.  $n = 6-7$  mice.

(H) Glucose disappearance rate during hyperinsulinemic-euglycemic clamp experiments performed on conscious, unrestrained control (white bars) and Vis-KO (red bars) mice after 8 weeks of HFD feeding.  $n = 5-6$  mice.

(I) 2-deoxyglucose uptake quantification of iWAT, gWAT, rWAT, and mWAT during hyperinsulinemic-euglycemic clamp experiments performed on conscious, unrestrained

876 control (white bars) and Vis-KO (red bars) mice after 8 weeks of HFD feeding. \* denotes  
877  $p < 0.05$  from unpaired Student's t-test. n = 5-6 mice.

878

**Figure 9. Adult mural cell deletion of *Zfp423* does not impact visceral white adipogenesis associated with high fat diet feeding.**

(A) Doxycycline (Dox) inducible deletion of *Zfp423* in adult mural cells (inducible-Mural-Knockout or “iMural-KO”) is achieved by breeding *Pdgfrb*<sup>rtTA</sup> transgenic mice to animals expressing Cre recombinase under the control of a tetracycline response element (*TRE-Cre*), the *Rosa26R loxP-mtdTomato-loxP-mGFP* (mT/mG) fluorescent reporter allele, and the floxed *Zfp423* alleles (*Zfp423*<sup>loxP/loxP</sup>). Animals carrying only *Pdgfrb*<sup>rtTA</sup>, *TRE-Cre*, and *Rosa26R*<sup>mT/mG</sup> alleles were used as controls.

(B) Validation of the iMural-KO model. Relative mRNA levels of *Zfp423* in purified adipocytes and purified *Pdgfrβ*<sup>+</sup> cells from WAT obtained from control (white bars) and iMural-KO (red bars) mice at 8 weeks of age. \* denotes p<0.05 from unpaired Student's t-test. n = 4-5 mice.

(C) Mice were maintained at room temperature and fed standard chow diet until 6 weeks of age. Animals were then switched to Dox-containing chow diet for 9 days in order to induce *Zfp423* deletion and mGFP expression in mural cells. Animals were then maintained on a Dox-containing high-fat diet (HFD) for 8 weeks then sacrificed for analysis.

(D) Weekly body weight measurements of control and iMural-KO mice during HFD feeding. n = 6-8 mice.

(E-J) Confocal images of immunostained gWAT obtained from control (E-G) and iMural-KO (H-J) mice fed high fat diet for 8 weeks.

(K) Quantification of mGFP-expressing adipocytes (mGFP<sup>+</sup>; perilipin<sup>+</sup>) observed in randomly chosen 10X magnification fields of gWAT sections obtained from control



902 (black circles) and iMural-KO (red squares) mice following 8 weeks of HFD feeding. n =  
903 6 mice.

904 (L) Glucose tolerance tests of control and iMural-KO mice after 8 weeks of HFD feeding.  
905 n = 6-8 mice.

906

**Figure 10. Inactivation of *Zfp423* in adult mural cells leads to beige, rather than white, adipocyte hyperplasia in diet-induced obesity.**

(A) Chow-fed 6 weeks-old animals were first administered Dox-containing chow for 9 days in order to inactivate *Zfp423* and induce permanent mGFP expression in *Pdgfrb*<sup>+</sup> cells. Mice were then switch to a high-fat diet (HFD) containing Dox. After 8 weeks of Dox-HFD, the mice were treated daily with CL316,243 (1 mg/kg/24h) or vehicle (PBS) for 4 weeks.

(B) Weekly body weight measurements of obese control and iMural-KO mice following vehicle or CL316,243 administration. n = 6-8 mice.

(C) Fat depot weights (normalized to body weight) of control and iMural-KO mice after vehicle or CL316,243 administration. \* denotes p<0.05 from unpaired Student's t-test. n = 6-8 mice.

(D-G) Representative confocal images of Perilipin (red), mGFP (green) and DAPI (blue) immunostaining of gWAT sections obtained from control and iMural-KO mice administered vehicle (D, E), or CL316,243 (F, G).

(H) Digital enhancement of region outlined in (G).

(I) Glucose tolerance tests of control and iMural-KO mice following vehicle or CL316,243 administration. \* denotes p<0.05 from unpaired Student's t-test. n = 6-8 mice.

(J) Serum insulin levels measured during intraperitoneal glucose tolerance tests of control and iMural-KO mice following vehicle or CL316,243 administration. n = 6-8 mice.

(K) Insulin tolerance tests of control and iMural-KO mice following vehicle or CL316,243 administration. \* denotes p<0.05 from unpaired Student's t-test. n = 6-8 mice.

**Figure 10- Supplement 1**

(A-B) Quantification of mGFP-expressing adipocytes (mGFP<sup>+</sup>; perilipin<sup>+</sup>) observed in randomly chosen 10X magnification fields of gWAT (A) or iWAT (B) sections of obese control and iMural-KO mice following vehicle or CL316,243 administration. n = 7 mice.

(C) Percentage of all perilipin<sup>+</sup> adipocytes counted in (A) that are multilocular. \* denotes p<0.05 from unpaired Student's t-test. n = 7 mice.

(D) Percentage of all perilipin<sup>+</sup> adipocytes counted in (B) that are multilocular. n = 7 mice.

(E) Relative mRNA levels of *Ucp1* in indicated WAT depots obtained from control and iMural-KO mice following vehicle or CL316,243 administration. \* denotes p<0.05 from unpaired Student's t-test. n = 6-8 mice.

(F) Relative basal oxygen consumption rates (OCRs) of isolated WAT depots from control and iMural-KO mice. \* denotes p<0.05 from unpaired Student's t-test. n = 4 independent replicates pooled from 2 mice.

**Table 1: qPCR primer sequences utilized for gene expression analysis**

<i>Gene</i>	Forward 5'-3'	Reverse 5'-3'
<i>Adipoq</i>	AGATGGCACTCCTGGAGAGAA	TTCTCCAGGCTCTCCTTTTCCT
<i>Adipsin</i>	CTACATGGCTTCCGTGCAAGT	AGTCGTCATCCGTCACTCCAT
<i>Cidea</i>	TCCTATGCTGCACAGATGACG	TGCTCTTCTGTATCGCCCAGT
<i>Cited1</i>	AACCTTGAGTGAAGGATCGC	GTAGGAGAGCCTATTGGAGATGT
<i>Dio2</i>	CATTGATGAGGCTCACCCCTTC	GGTTCCGGTGCTTCTTAACCT
<i>Ear2</i>	CCACAAAGCAGACAGGGAAAC	GCATGAGGCAAGCATTAGGAC
<i>Elovl3</i>	GTGTGCTTTGCCATCTACACG	CTCCCAGTTCAACAACCTTGC
<i>Fabp4</i>	GATGAAATCACCGCAGACGAC	ATTCCACCACCAGCTTGTCAC
<i>Foxo1</i>	GGCACTCCAAAACAGGACTTG	AAGAAATGGCAGAGGGAGGAG
<i>G6pc</i>	GGGCTGTTTGAGGAAAGTGTG	TATCCGACAGGAGGCTGGTAA
<i>Gsta3</i>	AGATCGACGGGATGAACTGG	CAGATCCGCCACTCCTTCT
<i>Hoxa9</i>	CCCCGACTTCAGTCCTTGC	GATGCACGTAGGGGTGGTG
<i>Lhx8</i>	GAGCTCGGACCAGCTTCA	TTGTTGTCTGAGCGAACTG
<i>Pck1</i>	TGTCTGTCCCATTGTCCACAG	AAGGTAAGGAAGGGCGGTGTA
<i>Pgc1α</i>	GCACCAGAAAACAGCTCCAAG	CGTCAAACACAGCTTGACAGC
<i>Pparg2</i>	GCATGGTGCCTTCGCTGA	TGGCATCTCTGTGTCAACCATG
<i>Prdm16</i>	ACACGCCAGTTCTCCAACCTGT	TGCTTGTTGAGGGAGGAGGTA
<i>Resistin</i>	AAGAACCTTTCATTTCCCCTCCT	GTCCAGCAATTTAAGCCAATGTT
<i>Rps18</i>	CATGCAAACCCACGACAGTA	CCTCACGCAGCTTGTTGTCTA
<i>Tcf21</i>	CCCTGAAAGTGGACTCCAACA	GCTGAGCGGGCTTTTCTTAGT
<i>Tle3</i>	GAGACTGAACACAATCCTAGCC	GGAGTCCACGTACCCCGAT
<i>Tmem26</i>	AGGGGCTTCCTTAGGGTTTTTC	CCGTCTTGATGAAGAAGCTG
<i>Ucp1</i>	TCTCAGCCGGCTTAATGACTG	GGCTTGCAATTCTGACCTTCAC
<i>Wt1</i>	ATAGGCCAGGGCATGTGTATG	CTGGTGCCTTGCTCTCTGATT
<i>Zfp423</i>	CAGGCCCAAGAAGAACAAG	GTATCCTCGCAGTAGTCGCACA
<i>Zic1</i>	CTGTTGTGGGAGACACGATG	CCTCTTCTCAGGGCTCACAG

**Table 2. Statistical Information**

Figure	N(sample size)	Statistical test method	Description		p-value
1B	Control n=6 Vis-KO n=6	Unpaired Student's t test	gWAT		4.56E-08
			mWAT		0.0019
			rWAT		0.0002
1D	Control n=6 Vis-KO n=6	Unpaired Student's t test	iWAT		0.0043
			gWAT		0.0051
1E	Control n=6 Vis-KO n=6	Unpaired Student's t test	iWAT	<i>Adipoq</i>	0.0111
			gWAT	<i>Adipsin</i>	0.004
1F	Control n=6 Vis-KO n=6	Unpaired Student's t test	iWAT	<i>Cidea</i>	0.012678087
				<i>Dio2</i>	0.015258263
				<i>Elovl3</i>	0.035976522
				<i>Prdm16</i>	0.043549713
			gWAT	<i>Cidea</i>	6.91848E-06
				<i>Dio2</i>	0.017046004
				<i>Prdm16</i>	9.5932E-05
			mWAT	<i>Cidea</i>	0.008754783
				<i>Dio2</i>	0.013198702
				<i>Prdm16</i>	0.018964447
			rWAT	<i>Cidea</i>	4.6109E-07
				<i>Dio2</i>	0.000934576
				<i>Prdm16</i>	0.000260661
1G	Control n=6 Vis-KO n=6	Unpaired Student's t test	iWAT		0.019621248
			gWAT		0.002534473
			mWAT		0.000189507
			rWAT		7.14636E-06

1H	Control n=4 Vis-KO n=4	Unpaired Student's t test	gWAT	Basal	0.02847
1I	Control n=4 Vis-KO n=4	Unpaired Student's t test	mWAT	Basal	0.00457
1J	Control n=4 Vis-KO n=4	Unpaired Student's t test	rWAT	Basal	0.04901
1K	Control n=4 Vis-KO n=4	Unpaired Student's t test	iWAT	Basal	0.03254
2B	Control n=4 Vis-KO n=4	Unpaired Student's t test	Inguinal	<i>Adipoq</i>	0.00251
2D	Control n=4 Vis-KO n=4	Unpaired Student's t test	Gonadal	<i>Zfp423</i>	2.1E-06
2E	Control n=4 Vis-KO n=4	Unpaired Student's t test	Gonadal	<i>Cidea</i> (red bar)	3.1573E-06
				<i>Cidea</i> (blue bar)	0.028888184
				<i>Dio2</i>	0.039314815
				<i>Ppargc1a</i>	0.00022784
				<i>Ucp1</i> (red bar)	0.004431674
				<i>Ucp1</i> (blue bar)	0.000356176
2F	Control n=4 Vis-KO n=4	Unpaired Student's t test	Gonadal	Basal	6.73733E-05
				Oligo.	0.000488801
				FCCP	0.02909696
2G	Control n=4 Vis-KO n=4	Unpaired Student's t test	Gonadal		0.03356
2H	Control n=4 Vis-KO n=4	Unpaired Student's t test	Gonadal	<i>Gsta3</i>	0.019517318
				<i>Tcf21</i>	0.014978261

				<i>Wt1</i>	0.000632618
				<i>Ear2</i>	0.009978141
				<i>Hoxa9</i>	0.000427928
				<i>Tmem26</i>	0.004299176
				<i>Zic1</i>	0.034783957
3A	Control n=5 Vis-KO n=4	Unpaired Student's t test	gWAT		0.000759641
			rWAT		0.001739073
3B	Control n=5 Vis-KO n=4			<i>Cidea</i>	0.000155141
				<i>Dio2</i>	0.009600651
				<i>Prdm16</i> (red bar)	0.002457629
				<i>Prdm16</i> (blue bar)	7.9394E-05
3G	Control n=5 Vis-KO n=4	Unpaired Student's t test	gWAT	<i>Gsta3</i>	0.044793954
				<i>Resistin</i>	0.002421899
				<i>Tmem26</i>	0.011651978
5A	Control n=5 Vis-KO n=4	Unpaired Student's t test	gWAT	<i>Ucp1</i>	0.011438323
			rWAT	<i>Ucp1</i>	0.001188624
5B	Control n=5 Vis-KO n=4	Unpaired Student's t test	rWAT	<i>Cidea</i>	0.000780591
				<i>Dio2</i>	0.002682038
				<i>Elovl3</i>	0.01642267
				<i>Prdm16</i> (red bar)	0.042213109
				<i>Prdm16</i> (blue bar)	0.000810897
			gWAT	<i>Dio2</i>	0.0221
				<i>Prdm16</i>	0.0127
5L	Control n=5 Vis-KO n=4	Unpaired Student's t test	t = 4 hours		0.014972958
			t = 5 hours		0.035138826

6D	Control n=7 Vis-KO n=6	Unpaired Student's t test	gWAT	<i>Zfp423</i>	0.002716658
			mWAT	<i>Zfp423</i>	0.042346922
			rWAT	<i>Zfp423</i>	0.018568608
6E	Control n=7 Vis-KO n=6	Unpaired Student's t test	iWAT	<i>Ucp1</i>	0.002716658
			gWAT	<i>Ucp1</i>	0.042346922
			rWAT	<i>Ucp1</i>	0.018568608
6F	Control n=7 Vis-KO n=6	Unpaired Student's t test	iWAT	<i>Cidea</i>	0.044864901
			gWAT	<i>Cidea</i>	0.011872021
				<i>Prdm16</i>	0.046343663
6H	Control n=4 Vis-KO n=4	Unpaired Student's t test	gWAT		0.00648
6I	Control n=4 Vis-KO n=4	Unpaired Student's t test	mWAT		0.03908
6J	Control n=4 Vis-KO n=4	Unpaired Student's t test	rWAT		0.03982
7D	Control n=4 Vis-KO n=5	Unpaired Student's t test	O <sub>2</sub> Consumption	24h	0.020700477
				Dark	0.006034333
7E	Control n=4 Vis-KO n=5	Unpaired Student's t test	Heat Production	24h	0.022957861
				Dark	0.007378241
7F	Control n=4 Vis-KO n=5	Unpaired Student's t test	CO <sub>2</sub> Production	24h	0.041576891
				Dark	0.017964281
8A	Control n=7 Vis-KO n=6	Unpaired Student's t test	t = 0 minutes		0.043779825
			t = 15 minutes		0.004769743
			t = 30 minutes		0.012903721
			t = 60 minutes		0.014915684
8B	Control n=7 Vis-KO n=6	Unpaired Student's t test	t = 0 minutes		0.009873322
			t = 30 minutes		0.01583899



8C	Control n=7 Vis-KO n=6	Unpaired Student's t test	t = 30 minutes		0.0426
8D	Control n=6 Vis-KO n=5	Unpaired Student's t test	Glucose Infusion Rate		0.04689
8E	Control n=6 Vis-KO n=5	Unpaired Student's t test	Hepatic Glucose Prod.	Basal	0.039627397
				Clamped	0.0346953
8F	Control n=7 Vis-KO n=6	Unpaired Student's t test	Liver	<i>Foxo1</i>	0.046418578
				<i>G6Pc</i>	0.024438785
				<i>Pck1</i>	0.047698079
8G	Control n=7 Vis-KO n=6	Unpaired Student's t test	TAG		0.02449
8I	Control n=4 Vis-KO n=5	Unpaired Student's t test	2-DG Uptake	rWAT	0.04023
9B	Control n=4 iMural-KO n=5	Unpaired Student's t test	Pdgfr $\beta$ cells		1.1E-05
10C	Control n=8 iMural-KO n=6	Unpaired Student's t test	gWAT		0.00276
10I	Control n=8 iMural-KO n=6	Unpaired Student's t test	t = 30 minutes		0.003328841
			t = 60 minutes		0.048919491
10K	Control n=8 iMural-KO n=6	Unpaired Student's t test	t = 15 minutes		0.03752
10-S1C	Control n=7 iMural-KO n=7	Unpaired Student's t test	gWAT		7.8E-08
10-S1E	Control n=8	Unpaired	iWAT	<i>Ucp1</i>	0.015960549

	iMural-KO n=6	Student's t test	gWAT	<i>Ucp1</i>	0.005703268
			rWAT	<i>Ucp1</i>	0.011883251
10-S1F	Control n=5	Unpaired Student's t test	iWAT		0.00019253
	Vis-KO n=5		gWAT		0.042623514
			mWAT		0.017424031
			rWAT		0.00228672

951

952

## References

- Bertholet, A.M., Kazak, L., Chouchani, E.T., Bogaczynska, M.G., Paranjpe, I., Wainwright, G.L., Betourne, A., Kajimura, S., Spiegelman, B.M., and Kirichok, Y. (2017). Mitochondrial Patch Clamp of Beige Adipocytes Reveals UCP1-Positive and UCP1-Negative Cells Both Exhibiting Futile Creatine Cycling. *Cell Metab* 25, 811-822 e814.
- Billon, N., and Dani, C. (2012). Developmental origins of the adipocyte lineage: new insights from genetics and genomics studies. *Stem Cell Rev* 8, 55-66.
- Chau, Y.Y., Bandiera, R., Serrels, A., Martinez-Estrada, O.M., Qing, W., Lee, M., Slight, J., Thornburn, A., Berry, R., McHaffie, S., *et al.* (2014). Visceral and subcutaneous fat have different origins and evidence supports a mesothelial source. *Nat Cell Biol* 16, 367-375.
- Chondronikola, M., Volpi, E., Borsheim, E., Porter, C., Annamalai, P., Enerback, S., Lidell, M.E., Saraf, M.K., Labbe, S.M., Hurren, N.M., *et al.* (2014). Brown adipose tissue improves whole-body glucose homeostasis and insulin sensitivity in humans. *Diabetes* 63, 4089-4099.
- Chondronikola, M., Volpi, E., Borsheim, E., Porter, C., Saraf, M.K., Annamalai, P., Yfanti, C., Chao, T., Wong, D., Shinoda, K., *et al.* (2016). Brown Adipose Tissue Activation Is Linked to Distinct Systemic Effects on Lipid Metabolism in Humans. *Cell Metab*.
- Cohen, P., Levy, J.D., Zhang, Y., Frontini, A., Kolodin, D.P., Svensson, K.J., Lo, J.C., Zeng, X., Ye, L., Khandekar, M.J., *et al.* (2014). Ablation of PRDM16 and beige adipose causes metabolic dysfunction and a subcutaneous to visceral fat switch. *Cell* 156, 304-316.
- Cohen, P., and Spiegelman, B.M. (2015). Brown and Beige Fat: Molecular Parts of a Thermogenic Machine. *Diabetes* 64, 2346-2351.
- Collins, S., Daniel, K.W., and Rohlf, E.M. (1999). Depressed expression of adipocyte beta-adrenergic receptors is a common feature of congenital and diet-induced obesity in rodents. *Int J Obes Relat Metab Disord* 23, 669-677.
- Collins, S., and Surwit, R.S. (2001). The beta-adrenergic receptors and the control of adipose tissue metabolism and thermogenesis. *Recent Prog Horm Res* 56, 309-328.
- Cypess, A.M., Weiner, L.S., Roberts-Toler, C., Franquet Elia, E., Kessler, S.H., Kahn, P.A., English, J., Chatman, K., Trauger, S.A., Doria, A., *et al.* (2015). Activation of human brown adipose tissue by a beta3-adrenergic receptor agonist. *Cell Metab* 21, 33-38.
- Cypess, A.M., White, A.P., Vernochet, C., Schulz, T.J., Xue, R., Sass, C.A., Huang, T.L., Roberts-Toler, C., Weiner, L.S., Sze, C., *et al.* (2013). Anatomical localization,

990 gene expression profiling and functional characterization of adult human neck brown fat.  
991 *Nat Med* 19, 635-639.

992 Gupta, R.K., Arany, Z., Seale, P., Mepani, R.J., Ye, L., Conroe, H.M., Roby, Y.A.,  
993 Kulaga, H., Reed, R.R., and Spiegelman, B.M. (2010). Transcriptional control of  
994 preadipocyte determination by Zfp423. *Nature* 464, 619-623.

995 Gupta, R.K., Mepani, R.J., Kleiner, S., Lo, J.C., Khandekar, M.J., Cohen, P., Frontini,  
996 A., Bhowmick, D.C., Ye, L., Cinti, S., *et al.* (2012). Zfp423 expression identifies  
997 committed preadipocytes and localizes to adipose endothelial and perivascular cells.  
998 *Cell Metab* 15, 230-239.

999 Harms, M., and Seale, P. (2013). Brown and beige fat: development, function and  
1000 therapeutic potential. *Nat Med* 19, 1252-1263.

1001 Hepler, C., and Gupta, R.K. (2017). The expanding problem of adipose depot  
1002 remodeling and postnatal adipocyte progenitor recruitment. *Mol Cell Endocrinol* 445, 95-  
1003 108.

1004 Hepler, C., Vishvanath, L., and Gupta, R.K. (2017). Sorting out adipocyte precursors  
1005 and their role in physiology and disease. *Genes Dev* 31, 127-140.

1006 Holland, W.L., Miller, R.A., Wang, Z.V., Sun, K., Barth, B.M., Bui, H.H., Davis, K.E.,  
1007 Bikman, B.T., Halberg, N., Rutkowski, J.M., *et al.* (2011). Receptor-mediated activation  
1008 of ceramidase activity initiates the pleiotropic actions of adiponectin. *Nat Med* 17, 55-63.

1009 Jeffery, E., Church, C.D., Holtrup, B., Colman, L., and Rodeheffer, M.S. (2015). Rapid  
1010 depot-specific activation of adipocyte precursor cells at the onset of obesity. *Nat Cell*  
1011 *Biol* 17, 376-385.

1012 Jeffery, E., Wing, A., Holtrup, B., Sebo, Z., Kaplan, J.L., Saavedra-Pena, R., Church,  
1013 C.D., Colman, L., Berry, R., and Rodeheffer, M.S. (2016). The Adipose Tissue  
1014 Microenvironment Regulates Depot-Specific Adipogenesis in Obesity. *Cell Metab* 24,  
1015 142-150.

1016 Kalinovich, A.V., de Jong, J.M., Cannon, B., and Nedergaard, J. (2017). UCP1 in  
1017 adipose tissues: two steps to full browning. *Biochimie* 134, 127-137.

1018 Karpe, F., and Pinnick, K.E. (2015). Biology of upper-body and lower-body adipose  
1019 tissue--link to whole-body phenotypes. *Nat Rev Endocrinol* 11, 90-100.

1020 Kiefer, F.W., Vernochet, C., O'Brien, P., Spoerl, S., Brown, J.D., Nallamshetty, S.,  
1021 Zeyda, M., Stulnig, T.M., Cohen, D.E., Kahn, C.R., *et al.* (2012). Retinaldehyde  
1022 dehydrogenase 1 regulates a thermogenic program in white adipose tissue. *Nat Med*  
1023 18, 918-925.

1024 Kim, J.Y., van de Wall, E., Laplante, M., Azzara, A., Trujillo, M.E., Hofmann, S.M.,  
1025 Schraw, T., Durand, J.L., Li, H., Li, G., *et al.* (2007). Obesity-associated improvements  
1026 in metabolic profile through expansion of adipose tissue. *J Clin Invest* 117, 2621-2637.

1027 Kissebah, A.H., Videlund, N., Murray, R., Evans, D.J., Hartz, A.J., Kalkhoff, R.K., and  
1028 Adams, P.W. (1982). Relation of body fat distribution to metabolic complications of  
1029 obesity. *J Clin Endocrinol Metab* 54, 254-260.

1030 Krotkiewski, M., Bjorntorp, P., Sjostrom, L., and Smith, U. (1983). Impact of obesity on  
1031 metabolism in men and women. Importance of regional adipose tissue distribution. *J*  
1032 *Clin Invest* 72, 1150-1162.

1033 Kusminski, C.M., Holland, W.L., Sun, K., Park, J., Spurgin, S.B., Lin, Y., Askew, G.R.,  
1034 Simcox, J.A., McClain, D.A., Li, C., *et al.* (2012). MitoNEET-driven alterations in  
1035 adipocyte mitochondrial activity reveal a crucial adaptive process that preserves insulin  
1036 sensitivity in obesity. *Nat Med* 18, 1539-1549.

1037 Lee, M.J., Wu, Y., and Fried, S.K. (2013). Adipose tissue heterogeneity: implication of  
1038 depot differences in adipose tissue for obesity complications. *Mol Aspects Med* 34, 1-  
1039 11.

1040 Lynes, M.D., Leiria, L.O., Lundh, M., Bartelt, A., Shamsi, F., Huang, T.L., Takahashi, H.,  
1041 Hirshman, M.F., Schlein, C., Lee, A., *et al.* (2017). The cold-induced lipokine 12,13-  
1042 diHOME promotes fatty acid transport into brown adipose tissue. *Nat Med*.

1043 Macotela, Y., Emanuelli, B., Mori, M.A., Gesta, S., Schulz, T.J., Tseng, Y.H., and Kahn,  
1044 C.R. (2012). Intrinsic differences in adipocyte precursor cells from different white fat  
1045 depots. *Diabetes* 61, 1691-1699.

1046 Manolopoulos, K.N., Karpe, F., and Frayn, K.N. (2010). Gluteofemoral body fat as a  
1047 determinant of metabolic health. *Int J Obes (Lond)* 34, 949-959.

1048 Morgan-Bathke, M., Chen, L., Oberschneider, E., Harteneck, D., and Jensen, M.D.  
1049 (2015). Sex and depot differences in ex vivo adipose tissue fatty acid storage and  
1050 glycerol-3-phosphate acyltransferase activity. *Am J Physiol Endocrinol Metab* 308,  
1051 E830-846.

1052 Ohlson, L.O., Larsson, B., Svardsudd, K., Welin, L., Eriksson, H., Wilhelmsen, L.,  
1053 Bjorntorp, P., and Tibblin, G. (1985). The influence of body fat distribution on the  
1054 incidence of diabetes mellitus. 13.5 years of follow-up of the participants in the study of  
1055 men born in 1913. *Diabetes* 34, 1055-1058.

1056 Rosen, E.D., and Spiegelman, B.M. (2014). What we talk about when we talk about fat.  
1057 *Cell* 156, 20-44.

1058 Rytko, J.M., Wueest, S., Schoenle, E.J., and Konrad, D. (2011). The portal theory  
1059 supported by venous drainage-selective fat transplantation. *Diabetes* 60, 56-63.

1060 Seale, P., Conroe, H.M., Estall, J., Kajimura, S., Frontini, A., Ishibashi, J., Cohen, P.,  
1061 Cinti, S., and Spiegelman, B.M. (2011). Prdm16 determines the thermogenic program of  
1062 subcutaneous white adipose tissue in mice. *J Clin Invest* 121, 96-105.

1063 Shao, M., Hepler, C., Vishvanath, L., MacPherson, K.A., Busbuso, N.C., and Gupta,  
1064 R.K. (2017). Fetal development of subcutaneous white adipose tissue is dependent on  
1065 Zfp423. *Mol Metab* 6, 111-124.

1066 Shao, M., Ishibashi, J., Kusminski, C.M., Wang, Q.A., Hepler, C., Vishvanath, L.,  
1067 MacPherson, K.A., Spurgin, S.B., Sun, K., Holland, W.L., *et al.* (2016). Zfp423  
1068 Maintains White Adipocyte Identity through Suppression of the Beige Cell Thermogenic  
1069 Gene Program. *Cell Metab*.

1070 Shinoda, K., Luijten, I.H., Hasegawa, Y., Hong, H., Sonne, S.B., Kim, M., Xue, R.,  
1071 Chondronikola, M., Cypess, A.M., Tseng, Y.H., *et al.* (2015). Genetic and functional  
1072 characterization of clonally derived adult human brown adipocytes. *Nat Med* 21, 389-  
1073 394.

1074 Stine, R.R., Shapira, S.N., Lim, H.W., Ishibashi, J., Harms, M., Won, K.J., and Seale, P.  
1075 (2016). EBF2 promotes the recruitment of beige adipocytes in white adipose tissue. *Mol*  
1076 *Metab* 5, 57-65.

1077 Svensson, K.J., Long, J.Z., Jedrychowski, M.P., Cohen, P., Lo, J.C., Serag, S., Kir, S.,  
1078 Shinoda, K., Tartaglia, J.A., Rao, R.R., *et al.* (2016). A Secreted Slit2 Fragment  
1079 Regulates Adipose Tissue Thermogenesis and Metabolic Function. *Cell Metab* 23, 454-  
1080 466.

1081 Thomou, T., Mori, M.A., Dreyfuss, J.M., Konishi, M., Sakaguchi, M., Wolfrum, C., Rao,  
1082 T.N., Winnay, J.N., Garcia-Martin, R., Grinspoon, S.K., *et al.* (2017). Adipose-derived  
1083 circulating miRNAs regulate gene expression in other tissues. *Nature* 542, 450-455.

1084 Tran, T.T., Yamamoto, Y., Gesta, S., and Kahn, C.R. (2008). Beneficial effects of  
1085 subcutaneous fat transplantation on metabolism. *Cell Metab* 7, 410-420.

1086 Vague, J. (1956). The degree of masculine differentiation of obesities: a factor  
1087 determining predisposition to diabetes, atherosclerosis, gout, and uric calculous  
1088 disease. *Am J Clin Nutr* 4, 20-34.

1089 van Marken Lichtenbelt, W.D., Vanhommerig, J.W., Smulders, N.M., Drossaerts, J.M.,  
1090 Kemerink, G.J., Bouvy, N.D., Schrauwen, P., and Teule, G.J. (2009). Cold-activated  
1091 brown adipose tissue in healthy men. *New England Journal of Medicine* 360, 1500-  
1092 1508.

1093 Villarroya, F., Cereijo, R., Villarroya, J., and Giralt, M. (2017). Brown adipose tissue as a  
1094 secretory organ. *Nat Rev Endocrinol* 13, 26-35.

1095 Virtanen, K.A., Lidell, M.E., Orava, J., Heglind, M., Westergren, R., Niemi, T., Taittonen,  
 1096 M., Laine, J., Savisto, N.J., Enerback, S., *et al.* (2009). Functional brown adipose tissue  
 1097 in healthy adults. *N Engl J Med* 360, 1518-1525.

1098 Vishvanath, L., MacPherson, K.A., Hepler, C., Wang, Q.A., Shao, M., Spurgin, S.B.,  
 1099 Wang, M.Y., Kusminski, C.M., Morley, T.S., and Gupta, R.K. (2016). Pdgfrbeta+ Mural  
 1100 Preadipocytes Contribute to Adipocyte Hyperplasia Induced by High-Fat-Diet Feeding  
 1101 and Prolonged Cold Exposure in Adult Mice. *Cell Metab* 23, 350-359.

1102 Vitali, A., Murano, I., Zingaretti, M.C., Frontini, A., Ricquier, D., and Cinti, S. (2012). The  
 1103 adipose organ of obesity-prone C57BL/6J mice is composed of mixed white and brown  
 1104 adipocytes. *J Lipid Res* 53, 619-629.

1105 Wang, Q.A., Tao, C., Gupta, R.K., and Scherer, P.E. (2013). Tracking adipogenesis  
 1106 during white adipose tissue development, expansion and regeneration. *Nat Med* 19,  
 1107 1338-1344.

1108 Wang, Q.A., Tao, C., Jiang, L., Shao, M., Ye, R., Zhu, Y., Gordillo, R., Ali, A., Lian, Y.,  
 1109 Holland, W.L., *et al.* (2015). Distinct regulatory mechanisms governing embryonic  
 1110 versus adult adipocyte maturation. *Nat Cell Biol* 17, 1099-1111.

1111 Wu, J., Bostrom, P., Sparks, L.M., Ye, L., Choi, J.H., Giang, A.H., Khandekar, M.,  
 1112 Virtanen, K.A., Nuutila, P., Schaart, G., *et al.* (2012). Beige adipocytes are a distinct  
 1113 type of thermogenic fat cell in mouse and human. *Cell* 150, 366-376.

1114 Yamamoto, Y., Gesta, S., Lee, K.Y., Tran, T.T., Saadatirad, P., and Kahn, C.R. (2010).  
 1115 Adipose depots possess unique developmental gene signatures. *Obesity (Silver Spring)*  
 1116 18, 872-878.

1117

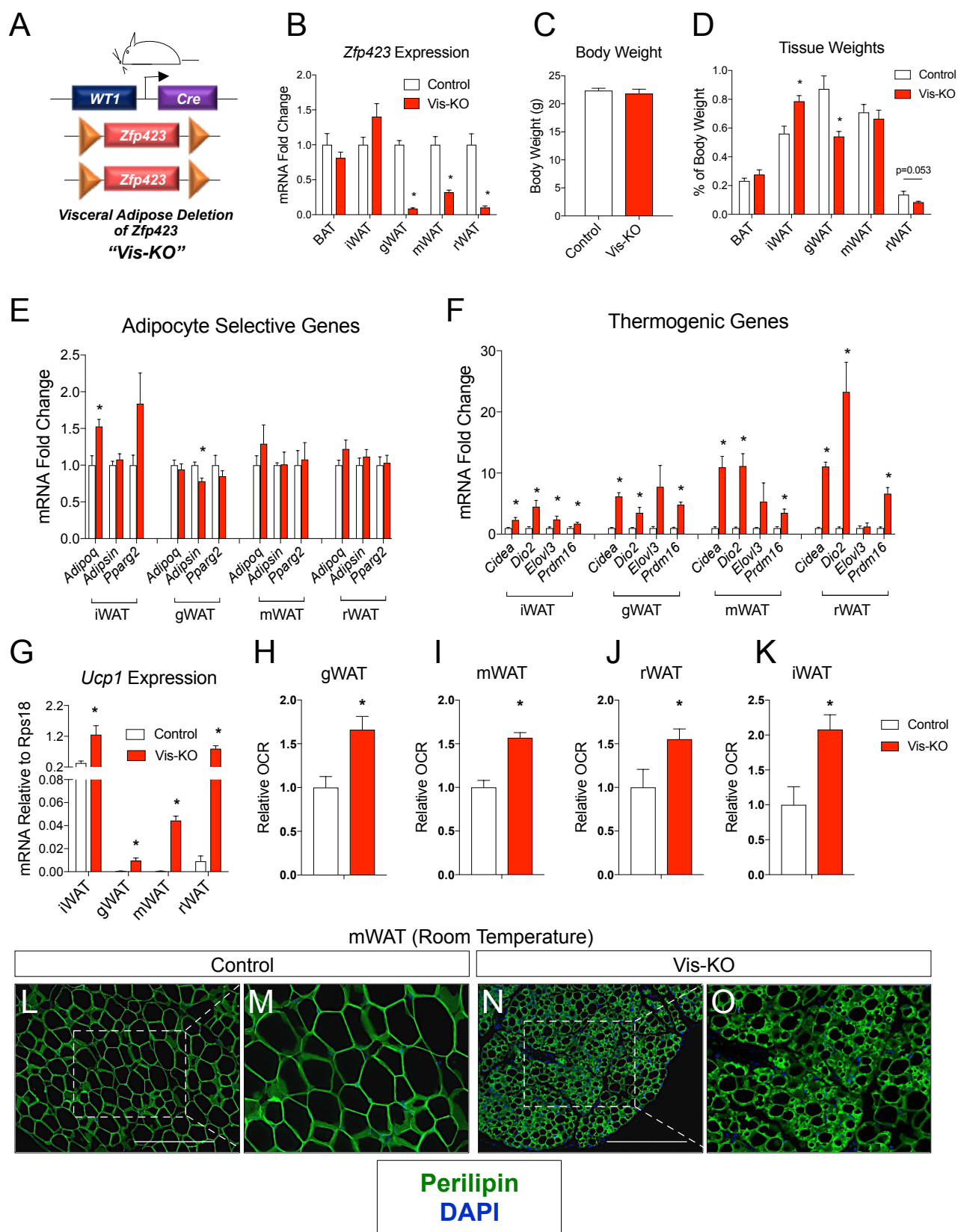


Figure 1



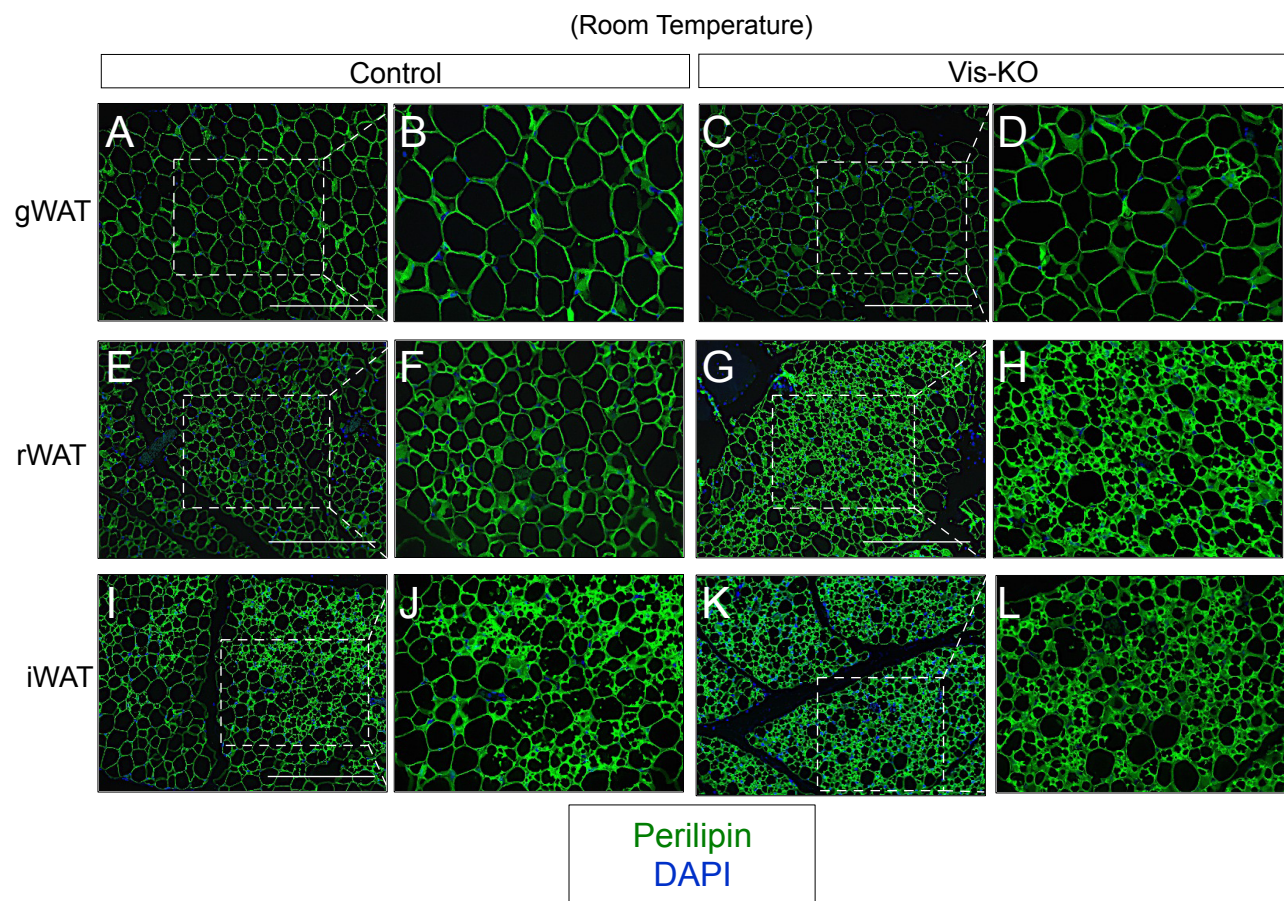


Figure 1- Supplement 1

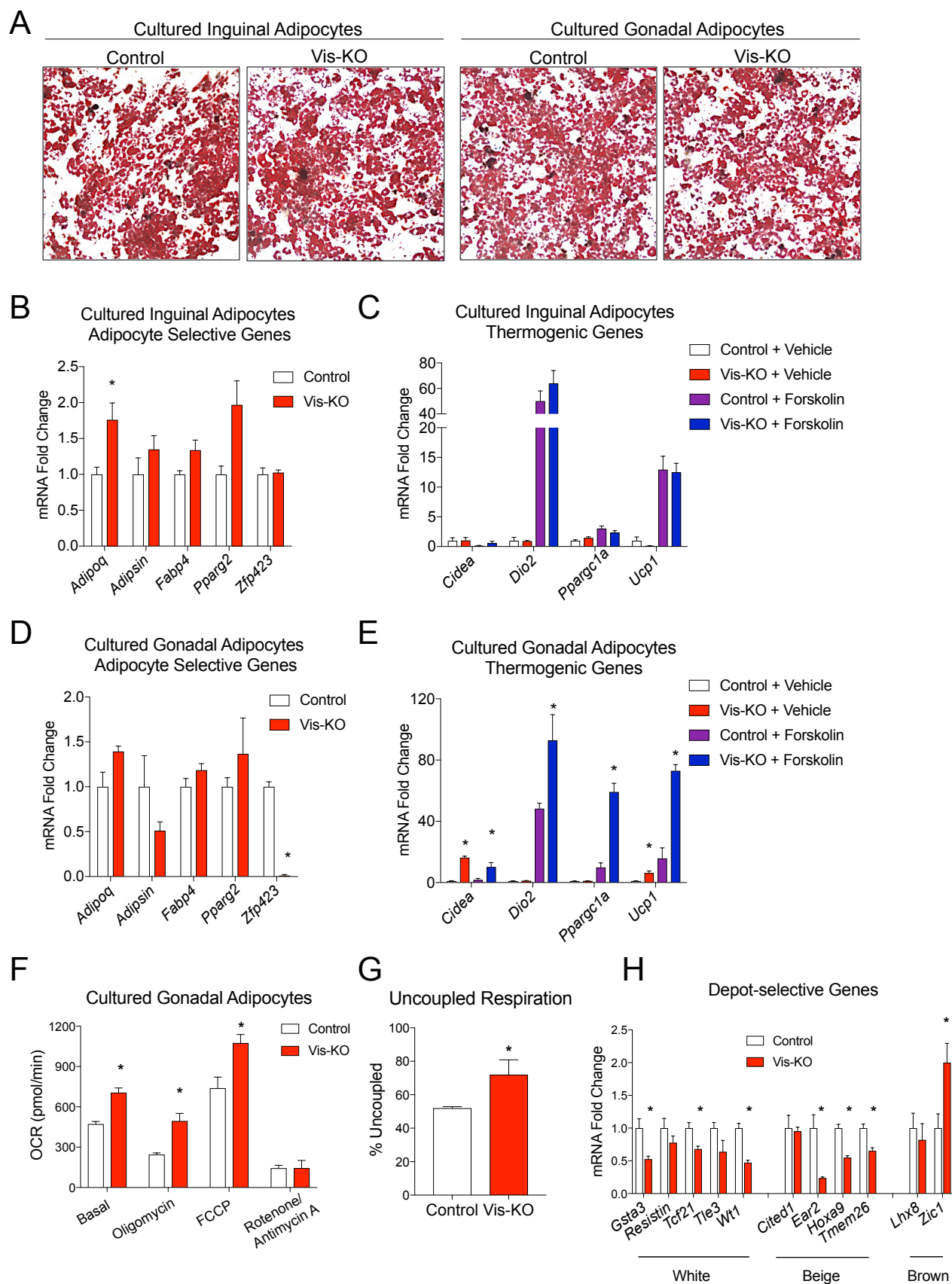
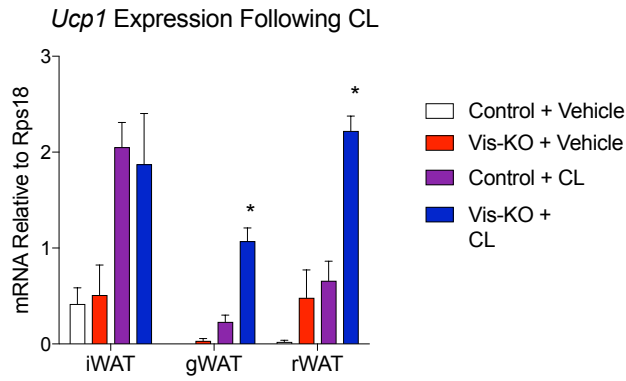
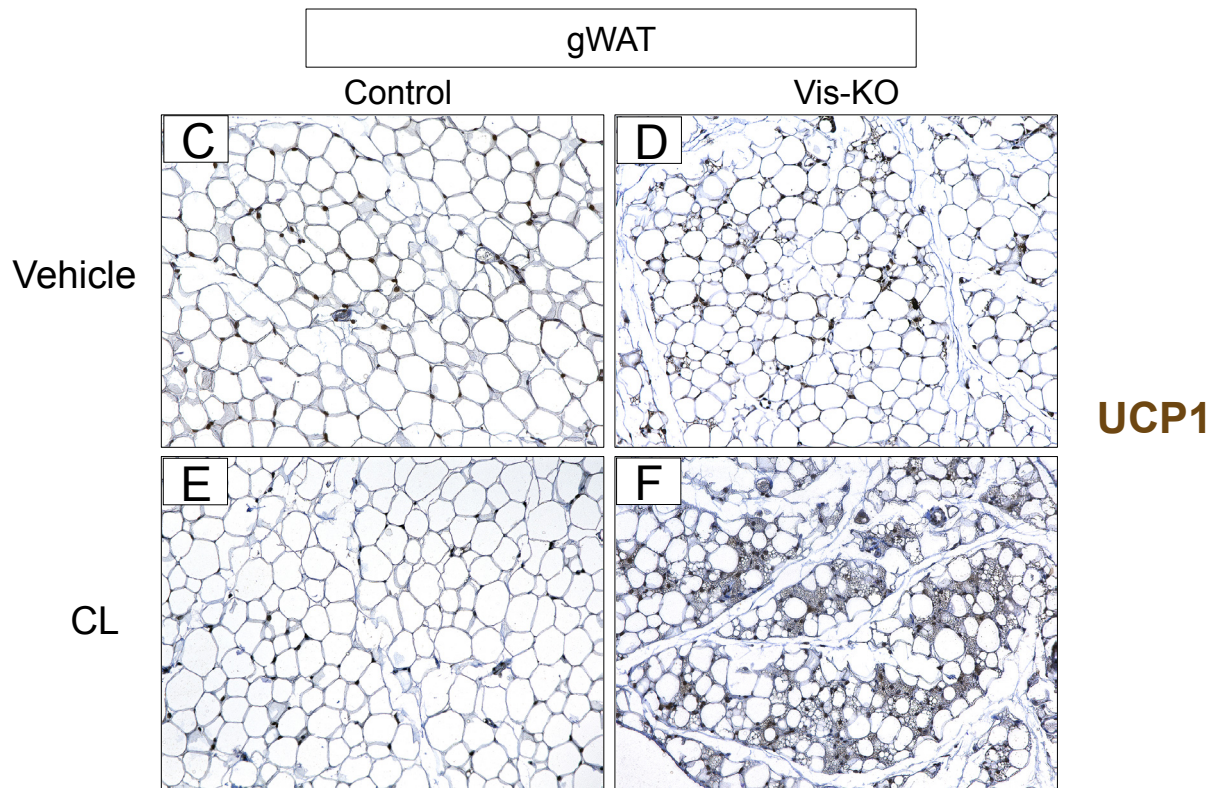
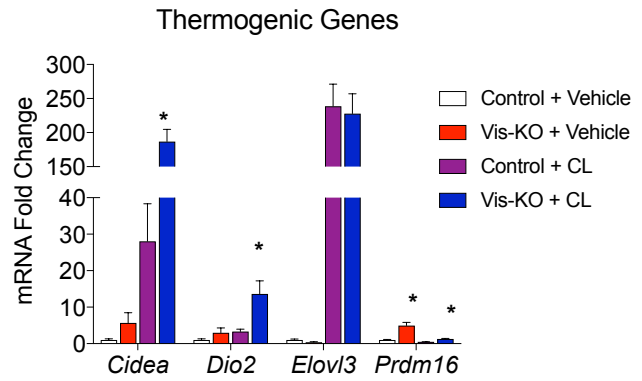


Figure 2

**A**



**B**



**G**

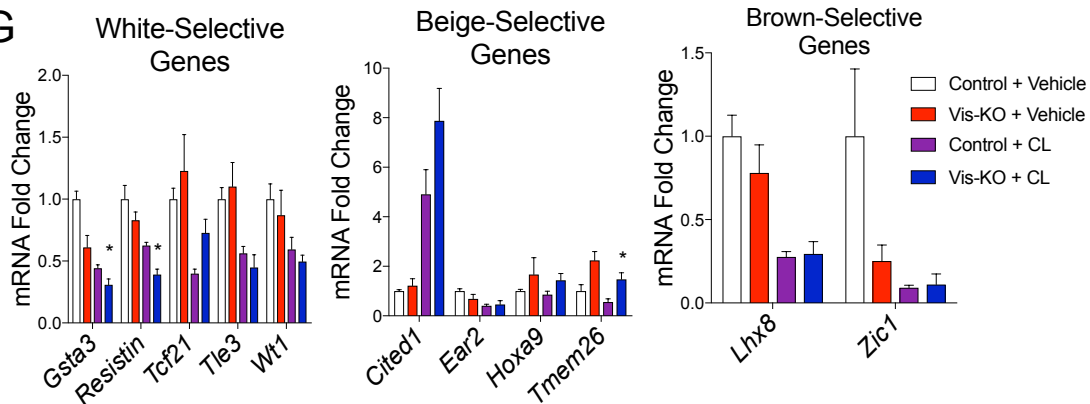


**Figure 3**



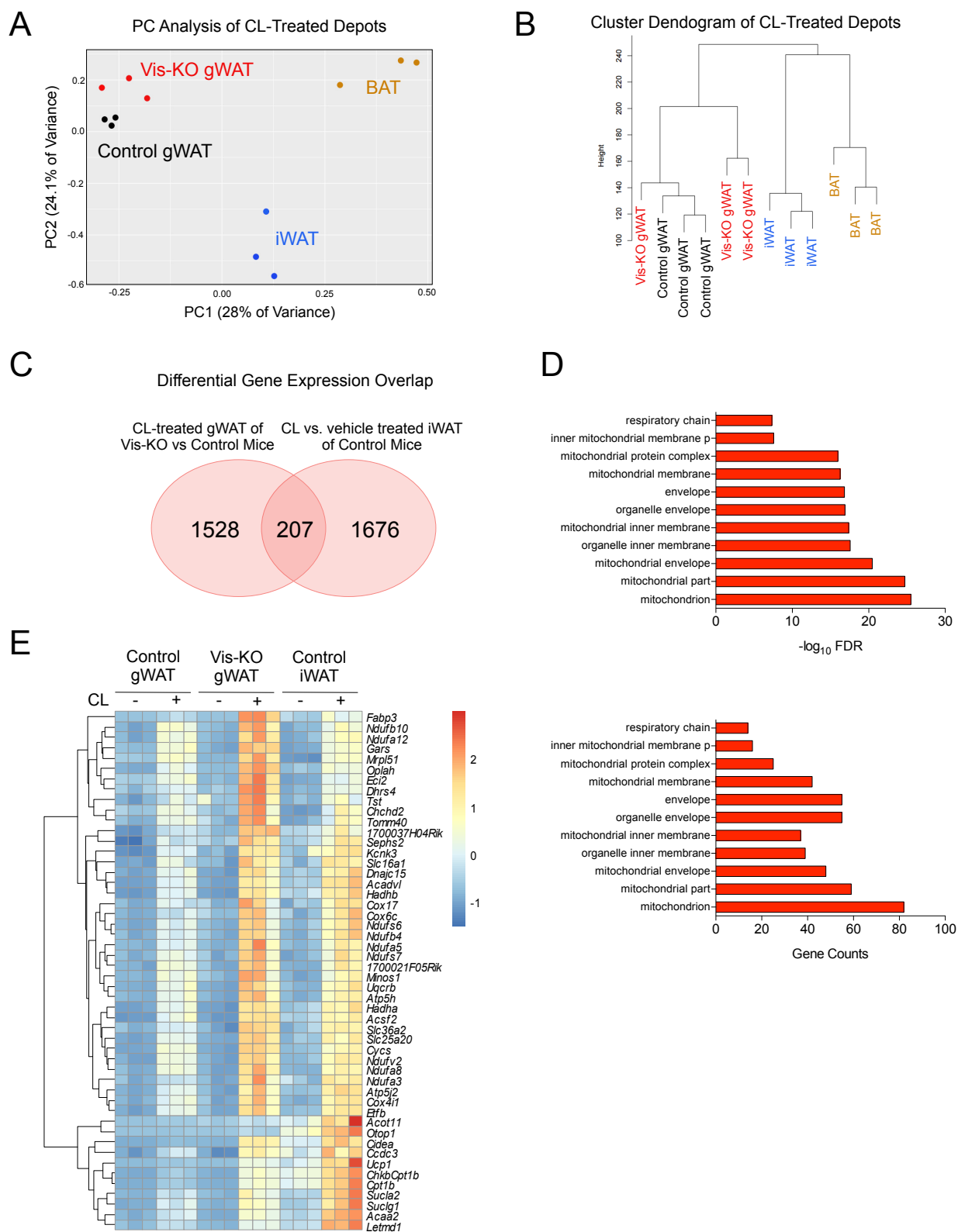


Figure 4

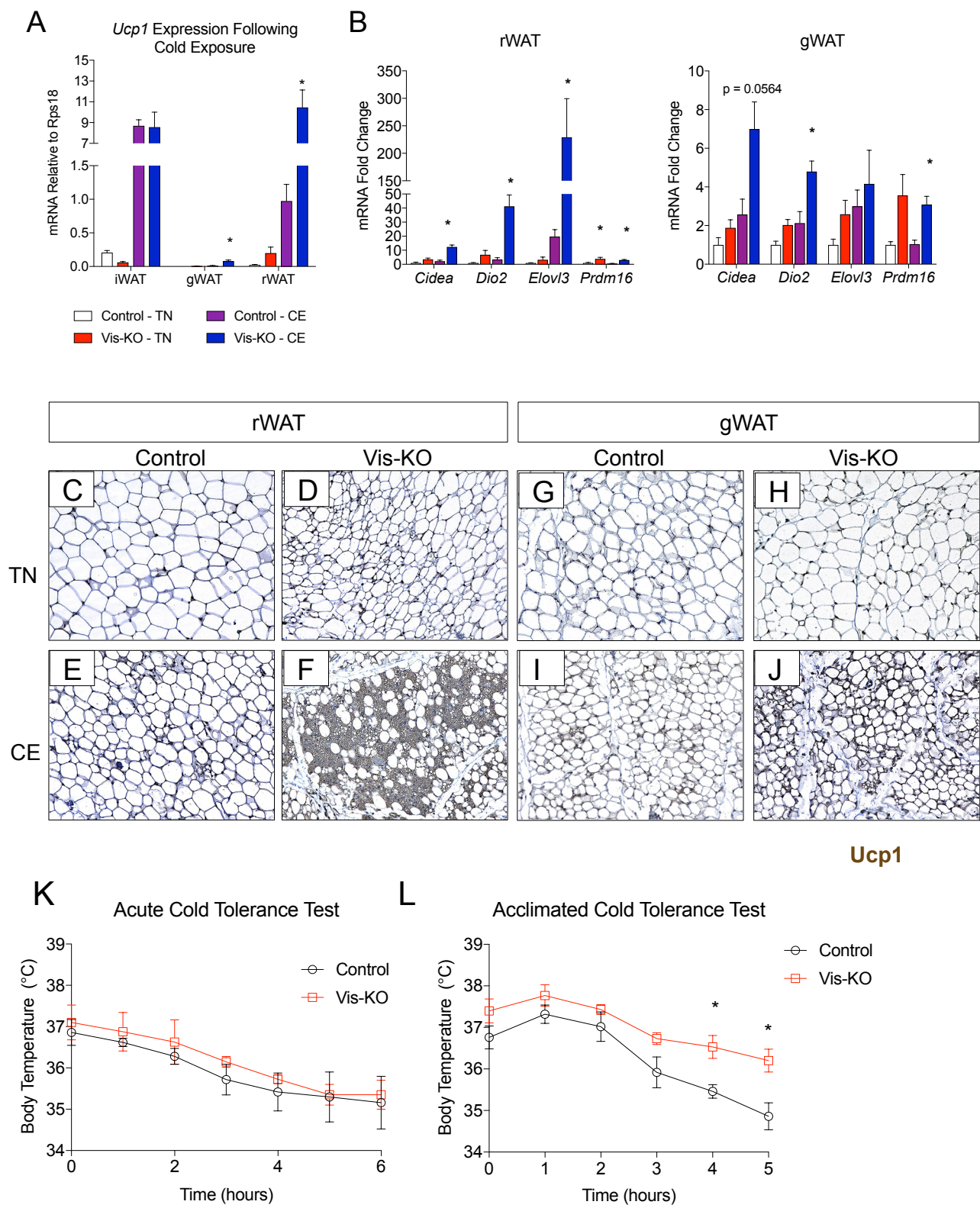


Figure 5

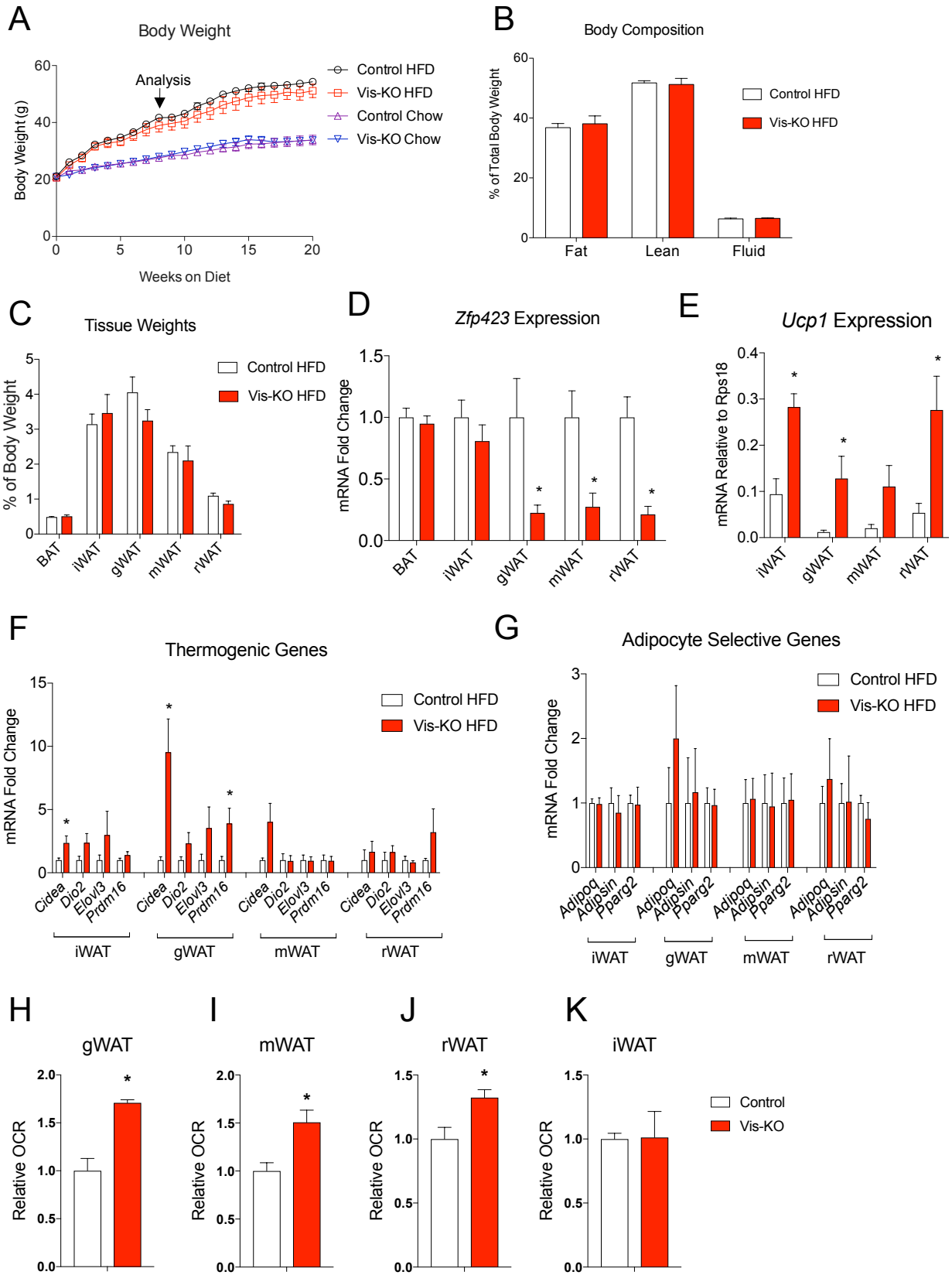


Figure 6

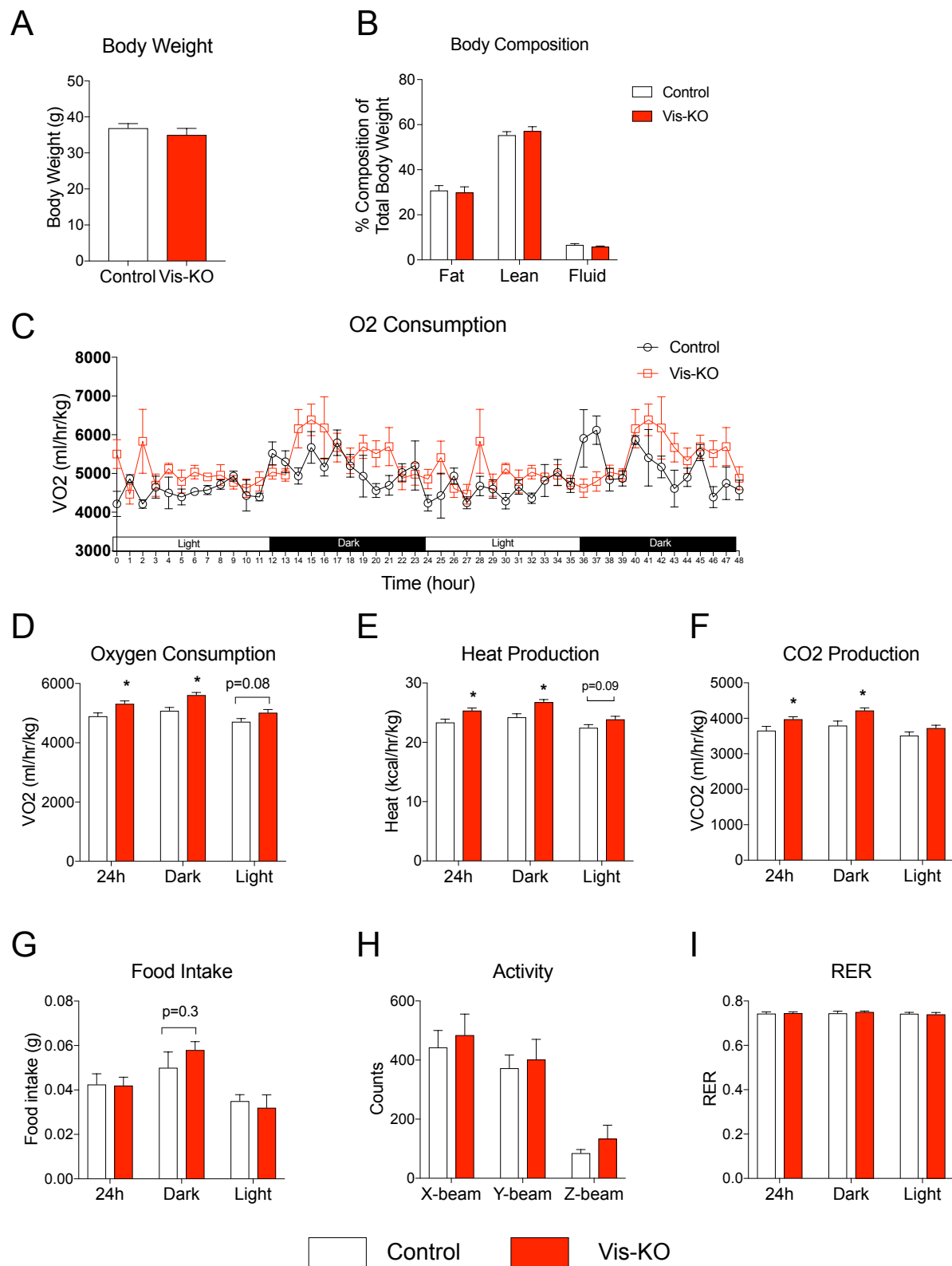


Figure 7

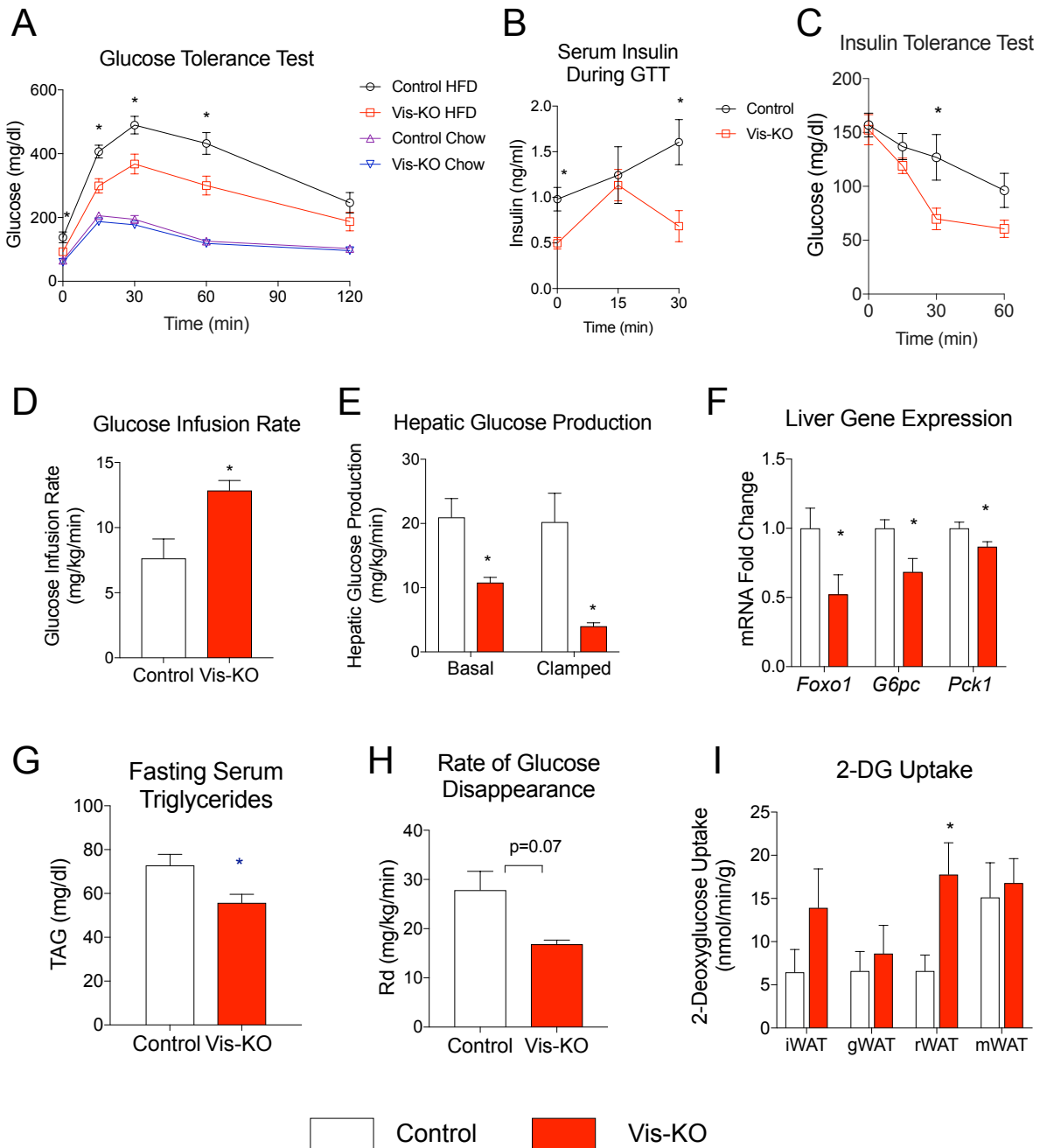


Figure 8



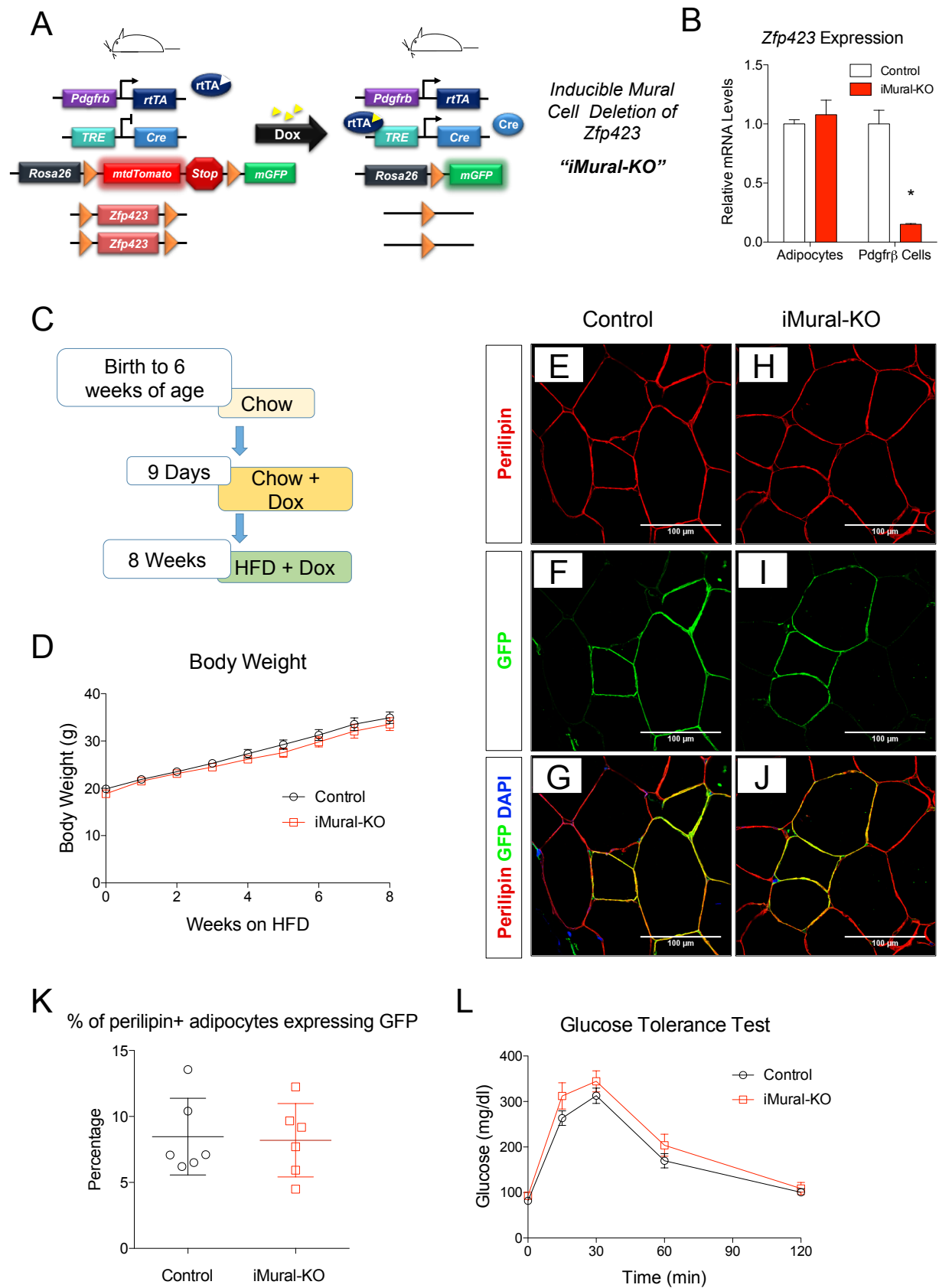


Figure 9

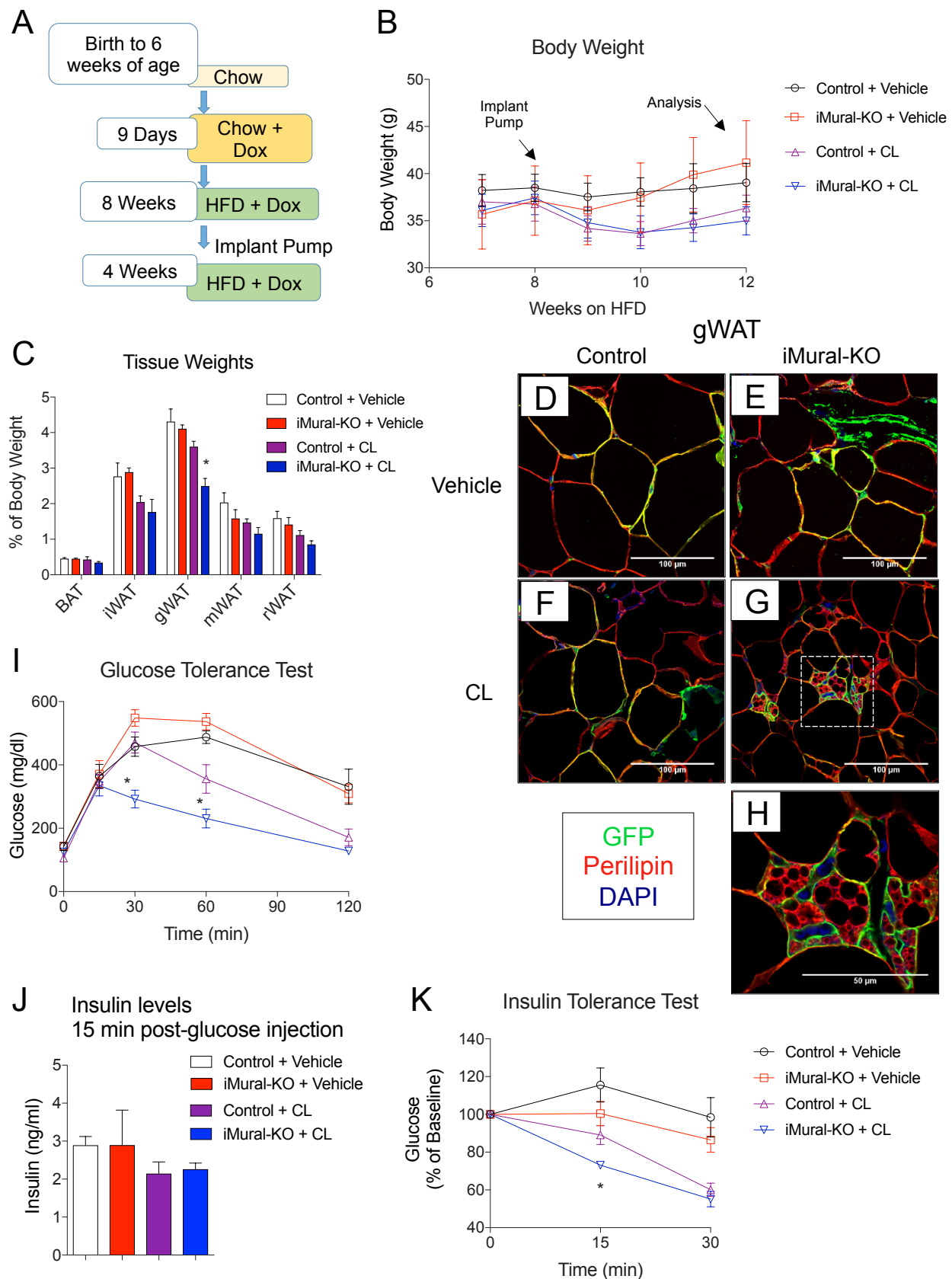


Figure 10

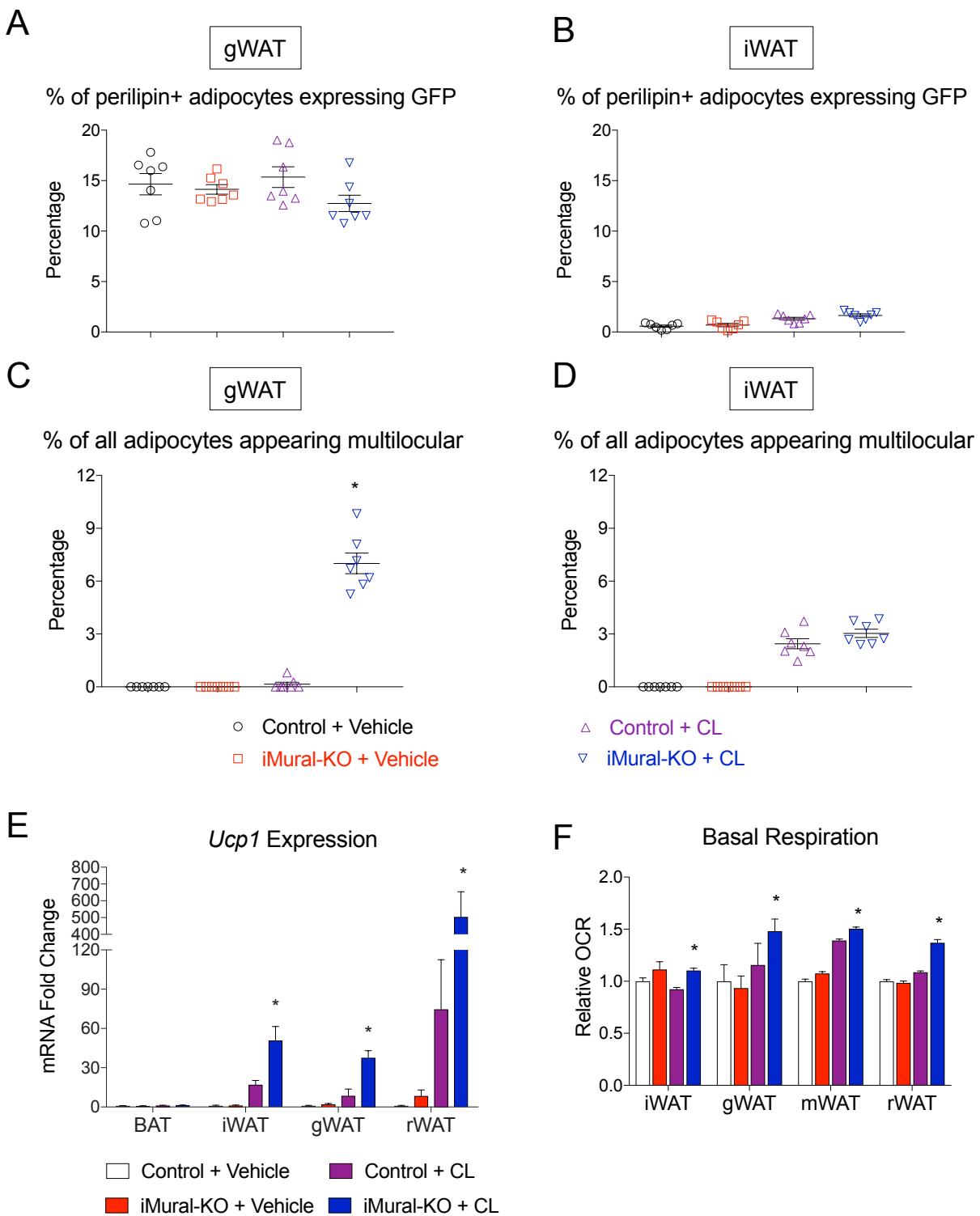


Figure 10- Supplement 1